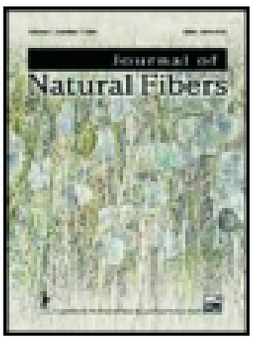

Journal of Natural Fibers

ISSN: (Print) (Online) Journal homepage: https://www.tandfonline.com/loi/wjnf20

Assessment of the Measurement and Prediction Methods for the Acoustic Properties of Natural Fiber Samples and Evaluation of Their Properties

Hasan Koruk

To cite this article: Hasan Koruk (2021): Assessment of the Measurement and Prediction Methods for the Acoustic Properties of Natural Fiber Samples and Evaluation of Their Properties, Journal of Natural Fibers, DOI: 10.1080/15440478.2021.1907835

To link to this article: https://doi.org/10.1080/15440478.2021.1907835

Published online: 20 Apr 2021.

JOURNAL OF NATURAL FIBERS
https://doi.org/10.1080/15440478.2021.1907835

Taylor & Francis
Taylor & Francis Group

REVIEW

Assessment of the Measurement and Prediction Methods for the Acoustic Properties of Natural Fiber Samples and Evaluation of Their Properties

Hasan Koruk

Mechanical Engineering Department, MEF University, Istanbul, Turkey

ABSTRACT

Although some studies have been conducted to show how natural fibers can replace synthetic materials, the use of many natural fibers is still limited. On the other hand, the use of natural fibers can become very common in many applications once their performance is fully understood. This paper aims to present a critical assessment of the acoustic properties of natural fiber samples. First, the methods commonly used for the measurement and prediction of the acoustic properties of natural fiber samples are determined. Second, the common techniques for measuring sound absorption coefficients (SACs) and sound transmission losses (STLs) are presented, and their advantages and limitations are evaluated. After that, the models commonly used for the prediction of acoustic properties are presented. Then, the SACs of many natural fiber samples are presented along with the thickness, bulk density and flow resistivity of the samples. Furthermore, the SACs of the samples are normalized using sample thickness and bulk density, and the sound absorption performance of the fiber samples is evaluated. Based on the results of many natural fiber samples, an empirical model for estimating the SACs of natural fiber samples is presented. Finally, the STLs of some porous natural fiber samples are presented.

摘要

虽然已经有一些研究表明天然纤维可以替代合成材料, 但许多天然纤维的使用仍然有限. 另一方面, 一旦对天然纤维的性能有了充分的了解, 天然纤维的使用在许多应用中就会变得非常普遍. 本文旨在对天然纤维样品的声学性能进行评价. 首先, 确定了天然纤维样品声学特性的常用测量和预测方法. 其次, 介绍了常用的吸声系数 (SACs) 和声传输损耗 (STLs) 测量技术, 并对其优缺点进行了评价. 在此基础上, 提出了常用的声学特性预测模型. 然后, 给出了许多天然纤维样品的SACs, 以及样品的厚度, 体积密度和流动电阻率. 此外, 利用样品厚度和体积密度对样品的声囊进行归一化处理, 评价了纤维样品的吸声性能. 基于大量天然纤维样品的实验结果, 提出了一种估算天然纤维样品SACs的经验模型. 最后, 给出了几种多孔天然纤维样品的STLs.

KEYWORDS

Natural fiber; acoustic properties; model; prediction; measurement; sound absorption; transmission loss

关键词

天然纤维; 声学性能; 模型; 测量; 吸声; 传输损耗

1. Introduction

Development of new materials to replace synthetic materials, such as carbon fibers, has become a necessity due to the adverse effects of chemical- or petroleum-based materials on nature and human health. Due to their biodegradability and sustainability, natural fibers are very promising alternatives to synthetic materials. Natural plant fibers include seed hairs (such as cotton), stem fibers (such as flax and hemp), leaf fibers (such as sisal) and husk fibers (such as coconut). Natural animal fibers include silk and wool. Although some studies have been conducted to show how natural fibers

*CONTACT Hasan Koruk korukh@mef.edu.tr Mechanical Engineering Department, MEF University, Istanbul, Turkey

can replace synthetic materials, or to reveal their applications (Das et al. 2020; Gurunathan, Mohanty, and Nayak 2015; Lalit, Mayank, and Ankur 2018; Steffens, Steffens, and Oliveira 2017; Sydow and Bienczak 2018; Wambua, Ivens, and Verpoest 2003), the use of many natural fibers is still limited. On the other hand, the use of natural fibers can become very common in many applications once their performance is fully understood. For example, natural fibers can even be used for the production of biodegradable face masks that are very critical to counter the coronavirus outbreak today (Das et al. 2020; Wibisono et al. 2020), and they can be widely exploited in many sound isolation applications (Lalit, Mayank, and Ankur 2018; Steffens, Steffens, and Oliveira 2017).

For the widespread use of natural fibers in practice, there is a need to evaluate the acoustic, mechanical and physical properties of these materials. In this study, a critical assessment of the acoustic properties of natural fiber samples is presented. The natural materials in this study include coconut, cotton, flax, hemp, jute, ramie and sisal fibers, which are the world's major plant fibers. In addition to these, date palm, esparto grass, kapok, kenaf and oil palm plant fibers are included in this study. Furthermore, the properties of sheep wool, glass wool and polyester fiber are included in the investigation for comparison purposes. For integrity, the methods for measuring and predicting the acoustic properties of natural fiber samples should be evaluated before presenting their acoustic properties. Therefore, first, the methods commonly used for the measurement and prediction of the acoustic properties of natural fiber samples were determined and listed in Table 1. The dimensions of the samples used in the tests, the frequency range covered and the standards specified in the studies are included in Table 1. For example, Oldham, Egan, and Cookson (2011), Xiang et al. (2013), Berardi, Iannace, and Di Gabriele (2017) and Santoni et al. (2019) used the two-microphone transfer function method to measure the acoustic properties of various natural fiber samples, including cotton, flax, jute, kapok, broom and hemp. It is clear that the two-microphone transfer function method is mostly used for the measurement of the sound absorption coefficients (SACs) of natural fiber samples, while the reverberation room chamber has been used in several studies. It seen that, although there are many studies on the SACs of natural fibers, there are only a few studies on the sound transmission losses (STLs) of natural fiber samples, and the four-microphone transfer matrix method is used in these studies (Bansod, Mittal, and Mohanty 2016; Bhingare and Prakash 2020; Chen and Jiang 2009; Kesharwani, Bedi, and Bahl 2020; Koruk and Genc 2015).

In addition to the experimental techniques, there are some mathematical models to predict or understand the sound absorption properties of porous natural fiber samples. For example, Fouladi, Ayub, and Nor (2011) used the Delany-Bazley and Biot-Allard models for the analysis of coir fiber samples. Oldham, Egan, and Cookson (2011) used the Delany-Bazley model for the prediction of the SACs of cotton, flax, jute and ramie fiber samples. Xiang et al. (2013) exploited the Garai-Pompoli model to predict the SACs of kapok fiber samples. Bansod, Mittal, and Mohanty (2016) used the Delany-Bazley-Miki and Johnson-Champoux-Allard models to analyze the acoustic properties of jute fiber samples. Berardi and Iannace (2017) discussed an inverse method for predicting the acoustical properties of different natural fibers, such as coconut, hemp, kenaf, and straw. Da Silva et al. (2019) used the Delany-Bazley and Johnson-Champoux-Allard models for the analysis of sisal fiber samples. Taban et al. (2020) used the Johnson-Champoux-Allard model to estimate the sound absorption performance of kenaf fiber samples. Liuzzi et al. (2020) used the Johnson-Champoux-Allard and Johnson-Champoux-Allard-Lafarge models to predict the sound absorption of some porous samples made from agricultural waste. Raj, Fatima, and Tandon (2020) exploited the Delany-Bazley-Miki and Garai-Pompoli models to predict the SACs of nettle fiber samples. It is seen that Delany-Bazley and Johnson-Champoux-Allard models are commonly used to predict the acoustic properties of natural fiber samples.

In this study, the methods that have been commonly used for both measuring and predicting the acoustic properties of natural fiber samples were determined, presented compactly and evaluated. Furthermore, the SACs of many natural fiber samples with different thicknesses, bulk densities and flow resistivities were presented, the SACs were normalized using the bulk density and thickness of the samples, and their sound absorption performance per unit mass was presented. Based on the

Table 1. The measurement and prediction methods for the acoustic properties of natural fiber samples.

Sample	Method for Measurement	Diameter (or Length x Width), mm	Frequency, Hz	Standard Mentioned	Model for Prediction	Reference
	Sound Absorption Coefficient					
Coconut Fiber	two-microphone transfer function	35	100–5000	ISO 10534–2 ASTM E1050	Delany-Bazley	Bhingare and Prakash 2020
		30 and 100	63–6300	ISO 10534–2	Delany-Bazley, Delany-Bazley-Miki and Johnson–Champoux–Allard	Taban et al. 2019c
		100	125–2000	ISO 10534–2	Delany-Bazley	Berardi and Iannace 2015
Cotton Fiber	two-microphone transfer function (and reverberation room)	29 and 100 (1000 x 1000)	50–6300	ISO 10534–2	Delany-Bazley and Garai-Pompoli	Oldham, Egan, and Cookson 2011
Date Palm Fiber	two-microphone transfer function	30 and 100	63–6300	ISO 10534–2	Delany-Bazley and Johnson–Champoux–Allard	Taban et al. 2019a
		30 and 100	63–6300	ISO 10534–2	Delany-Bazley and Johnson–Champoux–Allard	Taban et al. 2019b
Esparto Grass Fiber	two-microphone transfer function	40	200–3150	ISO 10534–2	Delany-Bazley	Arenas et al. 2020
Flax Fiber	two-microphone transfer function	29 and 100	50–6300	ISO 10534–2	Delany-Bazley and Garai-Pompoli	Oldham, Egan, and Cookson 2011
		16, 30 and 100	63–10000	ISO 10534–2	no prediction	Yang and Yan 2012
Hemp Fiber	two-microphone transfer function	100	125–2000	ISO 10534–2	Delany-Bazley	Berardi and Iannace 2015
		not available	100–5000	ISO 10534–2	Johnson–Champoux–Allard	Santoni et al. 2019
Jute Fiber	two-microphone transfer function (and reverberation room)	29 and 100 (1000 x 1000)	50–6300	ISO 10534–2	Delany-Bazley and Garai-Pompoli	Oldham, Egan, and Cookson 2011
	two-microphone transfer function	16, 30 and 100	63–10000	ISO 10534–2	Delany-Bazley and Garai-Pompoli	Yang and Yan 2012
		29 and 100	50–6400	ISO 10534–2	Delany-Bazley-Miki, Garai-Pompoli and Johnson–Champoux–Allard	Bansod, Mittal, and Mohanty 2016
Kapok Fiber	two-microphone transfer function	30 and 60	100–6300	ISO 10534–2	Garai-Pompoli	Xiang et al. 2013
Kenaf Fiber	two-microphone transfer function	100	125–2000	ISO 10534–2	Delany-Bazley	Berardi and Iannace 2015
	two-microphone transfer function (and reverberation room)	30–100 (3500 x 3500)	50–6300	ISO 10534 (and ISO 354)	Johnson–Champoux–Allard	Taban et al. 2020
Nettle Fiber	two-microphone transfer function	29 and 100	100–5000	ASTM E1050	Delany-Bazley-Miki and Garai-Pompoli	Raj, Fatima, and Tandon 2020
Oil Palm Fiber	two-microphone transfer function	28 and 100	50–4500	ASTM E1050	no prediction	Sambu et al. 2016

(*Continued*)

Table 1. (Continued).

Sample	Method for Measurement	Diameter (or Length x Width), mm	Frequency, Hz	Standard Mentioned	Model for Prediction	Reference
			Sound Absorption Coefficient			
Ramie Fiber	two-microphone transfer function (and reverberation room)	29 and 100 (1000 x 1000)	50–6300	ISO 10534–2	Delany-Bazley and Garai-Pompoli	Oldham, Egan, and Cookson 2011
	two-microphone transfer function	16, 30 and 100	63–10000	ISO 10534–2	no prediction	Yang and Yan 2012
Sisal Fiber	two-microphone transfer function	100	200–1600	ASTM E1050	Delany-Bazley and Johnson–Champoux–Allard	Da Silva et al. 2019
Jute Felt	two-microphone transfer function	29 and 100	50–6400	ISO 10534–2	Delany-Bazley-Miki, Garai-Pompoli and Johnson–Champoux–Allard	Bansod, Mittal, and Mohanty 2016
		29 and 100	50–6400	ISO 10534–2	Garai-Pompoli, Limp Frame and Johnson–Champoux–Allard	Bansod and Mohanty 2016
Sheep Wool	two-microphone transfer function (and reverberation room)	29 and 100 (1000 x 1000)	50–6300	ISO 10534–2	Delany-Bazley and Garai-Pompoli	Oldham, Egan, and Cookson 2011
	two-microphone transfer function	100	125–2000	ISO 10534–2	Delany-Bazley	Berardi and Iannace 2015
Glass Wool	two-microphone transfer function	40	100–5000	ISO 10534–2	Delany-Bazley and Delany-Bazley-Miki	Komatsu 2008
Polyester Fiber	two-microphone transfer function (and free-field impulse method)	-	100–6300	ISO 10534–2 (and ISO 10534–1)	Delany-Bazley and Dunn-Davern	Garai and Pompoli 2005
Sample			**Sound Transmission Loss**			
Coconut Fiber	four-microphone transfer matrix	35	100–5000	-	-	Bhingare and Prakash 2020
	*	30	150–12500	-	-	Kesharwani, Bedi, and Bahl 2020
Cotton & Ramie Fibers	four-microphone transfer matrix	29 and 100	100–6300	-	-	Chen and Jiang 2009
Hemp, Jute & Kenaf Fibers	*	30	150–12500	-	-	Kesharwani, Bedi, and Bahl 2020
Jute Felt	four-microphone transfer matrix	29 and 100	500–6400	ASTM E2611-09	Johnson–Champoux–Allard	Bansod, Mittal, and Mohanty 2016
Luffa Fiber	four-microphone transfer matrix	29	500–6000	-	-	Koruk and Genc 2015

normalized results of many natural fiber samples, an empirical model for the estimation of the SACs of porous samples was presented. In addition, the STLs of some porous natural fiber samples were presented in this study.

The structure of this paper is as follows. First, the techniques commonly used for the measurement of the acoustic properties of natural fiber samples are presented in Section 2. Here, the techniques for measuring both the SACs (Section 2.1) and STLs (Section 2.2) of natural fiber samples are included. The advantages and limitations of the common methods are summarized in Section 2.3. After that,

commonly used models to predict the SACs of natural fiber samples are presented in Sections 3.1.1–3.1.5. The estimation of the physical parameters needed in these models is presented in Section 3.1.6. The mathematical models for the prediction of the SACs of porous samples are evaluated in Section 3.1.7. The prediction of the STLs of structures is presented in Section 3.2. Subsequently, the SACs of many natural fibers are presented in Section 4.1. Both the SACs for 125–2000 Hz and the noise reduction coefficients (NRCs) of the samples are presented. Unlike some review studies in the literature, not only the SACs and thicknesses of the samples are presented, but also their bulk densities and flow resistivities are included. It should be noted that the SACs for different sample thickness, bulk density and flow resistivity values are presented in this study. In addition, by using the bulk density and thickness of the samples, the SACs are normalized, and the sound absorption performance of the samples per unit mass is presented. Furthermore, based on the normalized results of many natural fiber samples, an empirical model for the estimation of the SACs of porous samples is presented. It should be noted that, although there are various studies on the SACs of natural fiber samples (Bhingare, Prakash, and Vijaykumar 2019; Gokulkumar et al. 2020; Kalauni and Pawar 2019; Liao, Zhang, and Tang 2020; Mamtaz et al. 2016; Tang and Yan 2017; Yang et al. 2020), limited number of studies have included the STLs of these materials (Bansod, Mittal, and Mohanty 2016; Bhingare and Prakash 2020; Zhu et al. 2014). The STLs of some porous natural fiber samples are presented in Section 4.2. Finally, some concluding remarks are given in Section 5.

2. Measurement of acoustic properties

Once the methods commonly used to measure the SACs and STLs of natural fiber samples have been determined, they are presented and discussed here. The evaluations made here about the commonly used methods for measuring the acoustic properties of samples can be used to select the correct measurement technique, and to evaluate the measured results in real applications.

2.1. Measurement of sound absorption coefficients (SACs)

There are several methods for measuring the SACs of material samples, such as standing-wave-ratio method (or one-microphone impedance tube method), two-microphone transfer function method (or two-microphone impedance tube method), and reverberation room method. The two-microphone transfer function method is delineated in the ISO 10534–2 (ISO (International Organization for Standardization) 1998) and ASTM E1050 (ASTM (American Society for Testing and Materials) 2019a) standards. The reverberation room method is described in the ISO 354 (ISO (International Organization for Standardization) 2003) and ASTM C423 (ASTM (American Society for Testing and Materials) 2017) standards. As mentioned before, the researchers mostly used the two-microphone transfer function method, and there are several studies on the use of the reverberation room method to determine the SACs of natural fiber samples. Therefore, these two methods are presented below.

2.1.1. Two-microphone transfer function method

The schematic picture of the two-microphone transfer function method is shown in Figure 1. In this method, the complex-valued normal-incidence reflection coefficient R can be determined by (Koruk 2014):

$$R(\omega) = \frac{H_{12}(\omega) - e^{-jk_0 s}}{e^{jk_0 s} - H_{12}(\omega)} e^{2jk_0(s+L)} \tag{2.1}$$

where $\omega = 2\pi f$ is the angular frequency, $H_{12}(\omega)$ is the complex-valued acoustic transfer function, which is calculated from the sound pressure signals p_1 to p_2 measured with the two microphones, s is the distance between the two microphones, L is the distance between the right microphone and the test

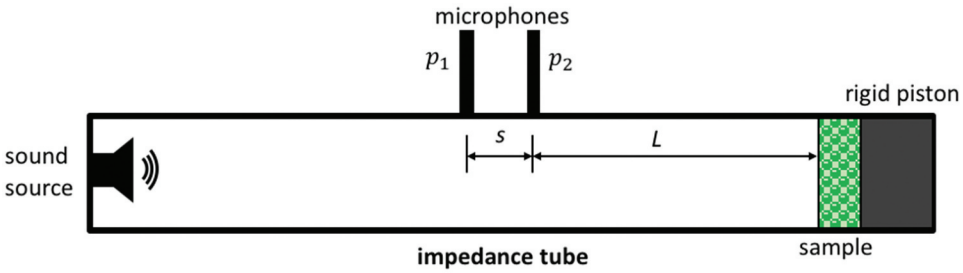

Figure 1. The schematic picture of the two-microphone transfer function method for the SAC measurements.

sample, $k_0 = \omega/c_0$ is the wave number of the air, where c_0 is the speed of the sound in the air, and $j = \sqrt{-1}$. The normal-incidence SAC is determined as:

$$\alpha(\omega) = 1 - |R(\omega)|^2 \tag{2.2}$$

2.1.2. Reverberation room method

The schematic drawing of the reverberation room method is shown in Figure 2. In this method, the random-incidence SAC is determined by (Shtrepi and Prato 2020):

$$\alpha_r(\omega) = \frac{1}{S}\left\{55.3V\left[\frac{1}{c_{02}t_2(\omega)} - \frac{1}{c_{01}t_1(\omega)}\right] - 4V(m_2 - m_1)\right\} \tag{2.3}$$

where S is the sample surface area (m^2), and V is the reverberation room volume (m^3). Here, $c_{01}$and c_{02} are the propagation speeds of sound in the air (m/s) without and with the test sample that can be calculated using $c_0 = 343.2\sqrt{293/T}$, where T represents the temperature (K); t_1 and t_2 are the reverberations times measured before and after the test sample is placed in the reverberation chamber or room; and $m_1$and m_2 are the power attenuation coefficients of the climatic conditions in the reverberation room without and with the samples that can be calculated according to ISO 9613–1 (ISO (International Organization for Standardization) 1993), respectively.

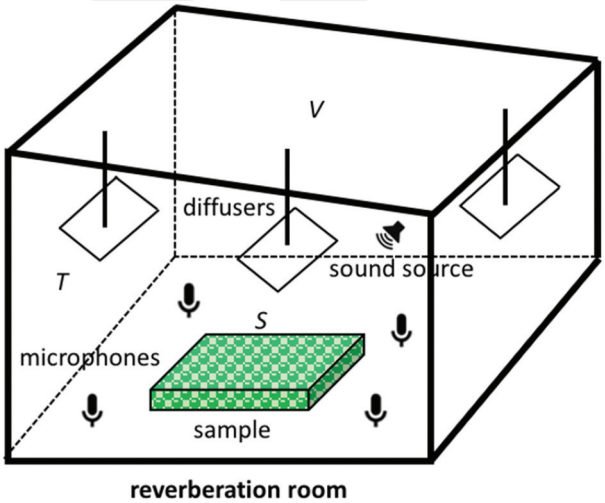

Figure 2. The schematic drawing of the reverberation room method for the SAC measurements.

2.2. Measurement of sound transmission losses (STLs)

There are various methods to measure the STLs of material samples, such as sound intensity method, four-microphone transfer matrix method, and conventional two-room method. The sound intensity method is delineated in the ISO 15186–1 standard (ISO (International Organization for Standardization) 2000). The four-microphone transfer matrix method is described in the ASTM E2611 standard (ASTM (American Society for Testing and Materials) 2019b). The conventional two-room method, in which both rooms are reverberant, is presented in the ASTM E90 standard (ASTM (American Society for Testing and Materials) 2016). It should be noted that, as mentioned earlier, the researchers mostly used the four-microphone transfer matrix method, and there are a few studies on the use of the conventional two-room method to experimentally determine the STLs of natural fiber samples. Therefore, after briefly mentioning the sound intensity method, the other two methods are presented below.

2.2.1. Sound intensity method

In the sound intensity method, in which the sample is placed between the source and receiving room, a microphone on the source side records the sound pressure levels, and an intensity mapping is obtained on the receiving side. The STL of the test sample is calculated using (Lai and Burgess 1991):

$$\mathrm{STL_r}(\omega) = L_{I_i}(\omega) - L_{I_t}(\omega) = L_{p_i}(\omega) - 6 - L_{I_t}(\omega) \tag{2.4}$$

where L_{p_i} is the incident space-averaged sound pressure level in the source room, and L_{I_i} and L_{I_t} are the incident and transmitted sound intensity levels, respectively. Although only one reverberant room is needed in this method, it is seen that this method is not common in practice today.

2.2.2. Four-microphone transfer matrix method

The schematic picture of the four-microphone transfer matrix method is shown in Figure 3. In this method, the sound pressures measured at four measurement positions, named x_1 to x_4, can be expressed as (Jung et al. 2008):

$$p_1 = Ae^{-jk_0x_1} + Be^{jk_0x_1} \tag{2.5a}$$

$$p_2 = Ae^{-jk_0x_2} + Be^{jk_0x_2} \tag{2.5b}$$

$$p_3 = Ce^{-jk_0x_3} + De^{jk_0x_3} \tag{2.5c}$$

$$p_4 = Ce^{-jk_0x_4} + De^{jk_0x_4} \tag{2.5d}$$

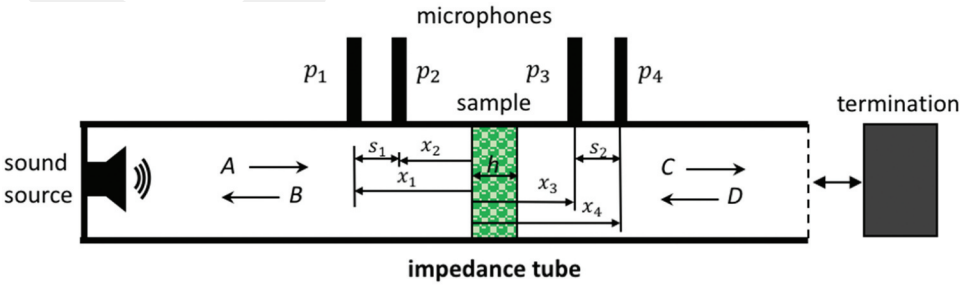

Figure 3. The schematic picture of the four-microphone transfer matrix method for the STL measurements.

where A and B indicate the incident and the reflected wave components in the upstream tube, and C and D show the transmitted and the reflected wave components in the downstream tube, respectively. The amplitudes A to D can be derived from the above equations as follows:

$$A = \frac{j\left(p_1 e^{jk_0 x_2} - p_2 e^{jk_0 x_1}\right)}{2\sin k_0 (x_1 - x_2)} \tag{2.6a}$$

$$B = \frac{j\left(p_2 e^{-jk_0 x_1} - p_1 e^{-jk_0 x_2}\right)}{2\sin k_0 (x_1 - x_2)} \tag{2.6b}$$

$$C = \frac{j\left(p_3 e^{jk_0 x_4} - p_4 e^{jk_0 x_3}\right)}{2\sin k_0 (x_3 - x_4)} \tag{2.6c}$$

$$D = \frac{j\left(p_4 e^{-jk_0 x_3} - p_4 e^{-jk_0 x_4}\right)}{2\sin k_0 (x_3 - x_4)} \tag{2.6d}$$

The problem can be formulated as the following matrix equation (Bolton, Yoo, and Olivieri 2007):

$$\begin{bmatrix} A \\ B \end{bmatrix} = \begin{bmatrix} T_{11} & T_{12} \\ T_{21} & T_{22} \end{bmatrix} \begin{bmatrix} C \\ D \end{bmatrix} \tag{2.7}$$

As Eq. (2.7) contains only two expressions but four unknowns (T_{11}, T_{12}, T_{21}, and T_{22}), it cannot be solved. Under certain circumstances, it is possible to exploit the reciprocal nature of a sample to generate two additional equations, instead of making a second set of measurements. It is noted that reciprocity requires that the determinant of the transfer matrix is unity ($T_{11}T_{22} - T_{12}T_{21} = 1$). Furthermore, we have $T_{11} = T_{22}$ for symmetrical systems (Bolton, Yoo, and Olivieri 2007). Now, let's consider a sample of depth h backed by a perfectly anechoic termination, so that it can be assumed that D is identically zero in the downstream tube section. Hence, the normal-incidence sound transmission coefficient $T_a = C/A$ is obtained as:

$$T_a(\omega) = \frac{2e^{jk_0 h}}{T_{11} + \frac{T_{12}}{\rho_0 c_0} + \rho_0 c_0 T_{21} + T_{22}} \tag{2.8}$$

Hence, the normal-incidence STL of a sample can be calculated as:

$$\mathrm{STL}(\omega) = 10\log\frac{1}{|T_a(\omega)|^2} = -20\log|T_a(\omega)| \tag{2.9}$$

Furthermore, if we use equal distance between the two microphones ($s_1 = s_2 = s$), STL can be written as follows (Jung et al. 2008):

$$\mathrm{STL}(\omega) = 20\log\left|\frac{e^{jk_0 s} - H_{12}(\omega)}{e^{jk_0 s} - H_{34}(\omega)}\right| - 20\log|H_t(\omega)| \tag{2.10}$$

where H_{12} and H_{34} are the acoustic transfer functions, which are calculated from the sound pressure levels p_1 to p_2 and p_3 to p_4, respectively, and $H_t = \sqrt{|S_d/S_u|}$ is the ratio between upstream (S_u) and downstream (S_d) auto-spectrums. It should be noted that the four-microphone transfer matrix method can be used to determine the SACs of test samples as well.

2.2.3. Conventional two-room method

The schematic drawing of the conventional two-room method is shown in Figure 4. In this method, in which both the source and receiving rooms are diffuse or reverberant, the STL of a partition with

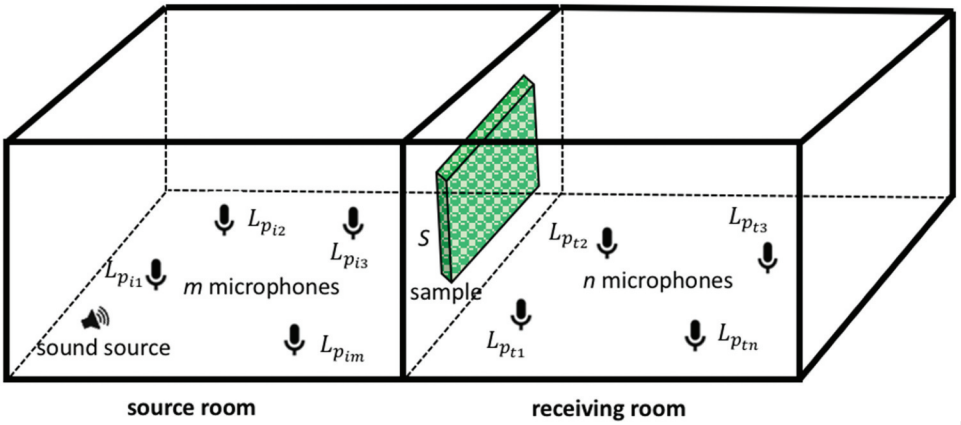

Figure 4. The schematic drawing of the conventional two-room method for the STL measurements.

surface area S can be expressed in terms of the average sound pressure level in the source room (L_{p_i}) and in the receiving room (L_{p_t}) as (Lai and Burgess 1991):

$$\mathrm{STL_r}(\omega) = L_{p_i}(\omega) - L_{p_t}(\omega) + 10\log[S/A(\omega)] \tag{2.11}$$

where A is the absorption of the receiving room.

2.3. Summarizing and comparing the common methods for measuring acoustic properties

Acoustic tests are performed using small cylindrical samples (about 15/30 to 100 mm in diameter) in the two-microphone transfer function (a) and four-microphone transfer matrix (b) methods, while larger samples (several meters in size) or complete objects are used in the reverberation room (c) and conventional two-room (d) methods. The first two methods (a and b) are widely used in practice, because impedance tubes are very suitable for laboratory measurements due to their small sizes, they require small-sized samples (limited wasted material), and the measurement time is short (a few minutes). However, with these two methods (a and b), only normal-incidence SACs and STLs in a limited frequency range that is imposed by tube dimensions (Koruk 2014) can be measured. Furthermore, the mounting condition of the test sample in the tubes can affect the SACs and STLs measured in these two methods (a and b).

The random incidences of sound wave in the reverberation room (c) and conventional two-room (d) methods are close to the practical conditions, therefore these methods (c and d) are considered to be superior to the other two methods (a and b). Furthermore, the SACs and STLs of test samples for a broad frequency range with limited edge effect can be obtained by these methods (c and d). However, these methods (c and d) require large samples (wasted material), and the working space for the rooms is much larger than the impedance tube facility that makes these methods impractical for laboratory measurements. Therefore, for example, small-scale reverberation rooms have been proposed to determine random-incidence SACs of test samples, but they have same drawbacks, such as edge effect and limited lower frequency range (Shtrepi and Prato 2020). The methods commonly used to measure the acoustic properties of material samples in practice and their advantages and disadvantages are presented in Figure 5.

3. Prediction of acoustic properties

After determining the commonly used models for the prediction of the SACs of natural fiber samples, these models are presented compactly and evaluated here. In addition, the prediction of the STLs of structures is presented. The evaluations made here about the common models for predicting the

Sound Absorption	Transmission Loss	Advantages	Disadvantages
a) Two-microphone transfer function method (ASTM E1050 & ISO 10534-2) 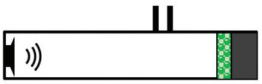	**b) Four-microphone transfer matrix method** (ASTM E2611) 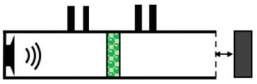	▪ Limited wasted material because of small test samples (3 to 10 cm in diameter) ▪ Practical for laboratory use because of small-sized test rigs ▪ Short measurement time durations (a few minutes)	▪ Only normal-incidence sound absorption coefficient and transmission loss measurements ▪ Limited frequency range imposed by tube dimensions ▪ Adverse effect of mounting condition of the sample in the tube (edge effect) ▪ Not possible to test large objects
c) Reverberation room method (ASTM C423 & ISO 354) 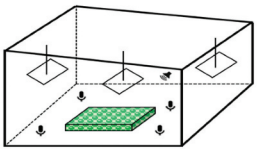	**d) Two-room method** (ASTM E90) 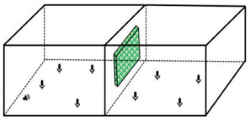	▪ Random-incidence sound absorption coefficient and transmission loss measurements ▪ Measurements for a broad frequency range ▪ Limited edge effect ▪ Possible to test large objects	▪ Huge amount of wasted material because of large samples (a few meters in length and width) ▪ Not practical for laboratory use because of large-sized test rigs ▪ Long measurement time durations

Figure 5. Four common methods to measure the acoustic properties of samples in practice.

acoustic properties of structures can be exploited to use the models correctly, and to assess the measured and predicted results in practice.

3.1. Prediction of sound absorption coefficients (SACs)

It is worth remembering that SAC is related to the reflection coefficient R as follows (Allard and Attala, 2009):

$$\alpha(\omega) = 1 - |R(\omega)|^2 \tag{3.1}$$

Therefore, we need to determine $R(\omega)$ to calculate $\alpha(\omega)$. The reflection coefficient at the surface of a layer is the ratio of the pressures created by the outgoing and ingoing waves at the surface of the layer. Having the surface acoustic impedance $Z(\omega)$, the reflection coefficient can be calculated by (Allard and Attala, 2009):

$$R(\omega) = \frac{Z(\omega) - Z_0}{Z(\omega) + Z_0} \tag{3.2}$$

where $Z_0 = \rho_0 c_0$ is the impedance of the air outside the material, c_0 is the speed of sound in the air, and ρ_0 is the density of the air. The surface acoustic impedance at normal incidence for a hard-backed sample with the thickness of h is given by (Kino 2015):

$$Z(\omega) = -j\frac{Z_c(\omega)}{\phi}\cot[k(\omega)h] \tag{3.3}$$

where ϕ is the porosity of the sample, and $k(\omega)$ is the wave number of the air in the sample. The characteristic impedance $Z_c(\omega)$ and the wave number $k(\omega)$, which are a function of frequency, can be estimated by the following equations (Kino 2015):

$$Z_c(\omega) = \sqrt{\rho(\omega)K(\omega)} \tag{3.4}$$

$$k(\omega) = \omega\sqrt{\frac{\rho(\omega)}{K(\omega)}} \tag{3.5}$$

where $\rho(\omega)$ and $K(\omega)$ are the so-called dynamic density and bulk modulus of the air in the sample. It is seen that we need (a) k (or ρ and K) and (b) Z_c to calculate α. There are different methods to determine these parameters in the literature. As mentioned before, the researchers mostly used the Delany-Bazley model as well as its modified versions and Johnson-Champoux-Allard model to predict the acoustic properties of natural fiber samples.

3.1.1. Delany-Bazley model

The Delany-Bazley model (Delany and Bazley 1970) is a relatively simple technique for the estimation of the acoustic parameters of a layer of isotropic and homogenous porous material. This model allows to replace a layer of fibrous material, with porosity close to one ($\phi \approx 1$), by a layer of equivalent fluid. The complex wave number k and the characteristic impedance Z_c were measured by Delany and Bazley (1970) for a large range of frequencies using many fibrous samples with porosity close to unity (Allard and Attala, 2009). According to these measurements, the quantities k and Z_c depend mainly on the frequency ω and on the flow resistivity σ of the porous media. A proper fit of the measured values of k and Z_c was obtained with the following expressions (Progneaux, Bouillard, and Deraemaeker 2015):

$$Z_c(\omega) = Z_0\left\{\left[1 + c_1\left(\frac{\omega}{2\pi\sigma}\right)^{c_2}\right] - jc_3\left(\frac{\omega}{2\pi\sigma}\right)^{c_4}\right\} \tag{3.6}$$

$$k(\omega) = k_0\left\{\left[1 + c_5\left(\frac{\omega}{2\pi\sigma}\right)^{c_6}\right] - jc_7\left(\frac{\omega}{2\pi\sigma}\right)^{c_8}\right\} \tag{3.7}$$

where $k_0 = \omega/c_0$ is the wave number of the air outside the sample, σ is the flow resistivity, and $c_1 - c_8$ are the Delany–Bazley regression constants (Table 2).

The importance of the Delany–Bazley model is its simplicity and application for a wide range of materials with $0.01 < \frac{\omega}{2\pi\sigma} < 1.0$ (Fouladi, Ayub, and Nor 2011). This empirical model can provide reasonable estimations of k and Z_c in the approximative frequency range defined by the relation $0.01 < \frac{\omega}{2\pi\sigma} < 1.0$, and it is widely used in practice for its simplicity (only one parameter, σ, is needed to describe the acoustic behavior of a porous sample).

3.1.2. Delany-Bazley-Miki model

After the work by Delany and Bazley (1970), several authors suggested slightly different empirical expressions of k and Z_c for specific frequency ranges and different porous samples (Dunn and Davern 1986; Miki 1990). In the case of multiple layers, Miki (1990) recognized that the real part of the surface impedance when computed with the Delany-Bazley model sometimes becomes negative at low frequencies (indicating a nonphysical result), and new coefficients were proposed. The so-called Delany-Bazley-Miki model has the same formula structure as the Delany-Bazley model; however, the coefficients (c_1, c_3, c_5 and c_7) and the degrees (c_2, c_4, c_6 and c_8) are different (Progneaux, Bouillard, and Deraemaeker 2015). The Delany-Bazley-Miki model regression constants are listed in Table 3.

Table 2. The Delany–Bazley model regression constants.

c_1	c_2	c_3	c_4	c_5	c_6	c_7	c_8
0.0497	−0.7540	0.0758	−0.7320	0.0858	−0.7000	0.1690	−0.5950

Table 3. The Delany-Bazley-Miki model regression constants.

c_1	c_2	c_3	c_4	c_5	c_6	c_7	c_8
0.0699	−0.6320	0.1070	−0.6320	0.1090	−0.6180	0.1600	−0.6180

3.1.3. Johnson-Champoux-Allard model

The geometry of fibrous samples was not considered in the Delany-Bazley model (Delany and Bazley 1970) and its modified versions (Dunn and Davern 1986; Miki 1990). A significant improvement in the description of the viscous forces was carried out by Johnson, Koplik, and Dashen (1987). Allard and Champoux (1992) obtained, from the geometry of the porous samples, new simple equations that give similar results in the range of validity of the equations of Delany and Bazley (1970), and they are based on a physical representation of the acoustical phenomena associated with the different physical properties of the porous materials. The so-called Johnson-Champoux-Allard model (Allard and Champoux 1992) is a rigid-frame model, where the solid phase of the frame remains motionless. In addition to the static air flow resistivity (σ) used in the Delany-Bazley model and its modified versions, the open porosity, high-frequency limit of tortuosity (α_∞), viscous characteristic length (Λ), and thermal characteristic length (Λ') are used in this model. It should be noted that Λ and Λ' relate the viscous and thermal losses, respectively (Fouladi, Ayub, and Nor 2011).

In order to take into account the inertial and the viscous couplings between the air and the frame in an air-saturated rigid-frame porous sample, the equilibrium density ρ_0 is replaced by the dynamic density $\rho(\omega)$ that depends on frequency in the Johnson-Champoux-Allard model (Allard and Champoux 1992). Dynamic density that is proposed by Johnson, Koplik, and Dashen (1987) is given by (Allard and Champoux 1992; Kino 2015; Kino and Ueno 2008):

$$\rho(\omega) = \rho_0 \alpha_\infty \left(1 + \frac{\sigma\phi}{j\alpha_\infty \rho_0 \omega}\sqrt{1 + \frac{4j\alpha_\infty^2 \eta \rho_0 \omega}{\sigma^2 \Lambda^2 \phi^2}}\right) \tag{3.8}$$

where η is the viscosity of air. The tortuosity relates $\rho(\omega)$ and ρ_0 according to (Allard and Champoux 1992):

$$\lim_{\omega \to \infty} \rho(\omega) = \rho_0 \alpha_\infty \tag{3.9}$$

In the case of cylindrical pores making an angle θ with the direction of propagation, α_∞ is equal to (Allard and Champoux 1992):

$$\alpha_\infty = \frac{1}{\cos^2(\theta)} \tag{3.10}$$

The viscous characteristic length introduced by Johnson, Koplik, and Dashen (1987) is given by (Allard and Champoux 1992):

$$\Lambda = \frac{2\int_V |v(\mathbf{r})|^2 dV}{\int_A |v(\mathbf{r}_\omega)|^2 dA} \tag{3.11}$$

where the integral in the numerator is evaluated over the volume of the pore, and $v(\mathbf{r})$ is the velocity of an inviscid fluid in the pore. The integral in the denominator is taken over the surface of the pore, and $v(\mathbf{r}_\omega)$ is the velocity of the same inviscid fluid at the surface of the pore wall.

Champoux and Allard (1991) presented an expression for the dynamic bulk modulus for the same porous sample based on the previous study (Johnson, Koplik, and Dashen 1987) given by (Kino 2015; Kino and Ueno 2008):

$$K(\omega) = \frac{\gamma P_0}{\gamma - (\gamma - 1)\left(1 + \frac{8\eta}{j\Lambda'^2 \rho_0 P_r \omega}\sqrt{1 + \frac{j\rho_0 \Lambda'^2 P_r \omega}{16\eta}}\right)^{-1}} \tag{3.12}$$

where P_0 is the atmospheric pressure, γ is the specific heat ratio of the air, and P_r is the Prandtl number of the air. The thermal characteristic length is given by (Allard and Champoux 1992):

$$\Lambda' = \frac{2\int_V dV}{\int_A dA} \tag{3.13}$$

It should be noted that the equation of Λ' is equivalent to the equation of Λ without the squared velocity weighting (Allard and Champoux 1992).

3.1.4. Johnson-Champoux-Allard-Lafarge model

The Johnson-Champoux-Allard-Lafarge model is based on the study by Johnson, Koplik, and Dashen (1987) to describe viscous and inertial dissipative effects inside the porous sample and the studies by Champoux and Allard (1991) and Lafarge et al. (1997) to describe the thermal dissipative effects. The dynamic density used in this model is the same as the one for the Johnson-Champoux-Allard model given in Eq. (3.8). Different from the Johnson-Champoux-Allard model, the thermal static permeability (q_0') is used for the low-frequency behavior of thermal effects in the Johnson-Champoux-Allard -Lafarge model (Lafarge et al. 1997). As a result, the dynamic bulk modulus is given as:

$$K(\omega) = \frac{\gamma P_0}{\gamma - (\gamma - 1)\left[1 - j\frac{\phi\kappa}{q_0' c_p \rho_0 \omega}\sqrt{1 + j\frac{4q_0'^2 c_p \rho_0 \omega}{\kappa \Lambda'^2 \phi^2}}\right]^{-1}} \tag{3.14}$$

where c_p is the specific heat of the air at constant pressure, and κ is the thermal conductivity of the air.

3.1.5. Biot-Allard model

In addition to the parameters used in the Johnson-Champoux-Allard-Lafarge model, the Biot-Allard model takes into account the loss factor (η_s), density (ρ_s), Poisson's ratio (ν_s) and Young's modulus (E_s) of the frame of the porous sample (Allard and Atalla, 2009). Overall, in this model, the surface impedance is calculated using (Allard and Atalla, 2009; Fouladi, Ayub, and Nor 2011):

$$Z = -j\frac{\left(Z_1^s Z_2^a \zeta_2 - Z_2^s Z_1^a \zeta_1\right)}{D} \tag{3.15}$$

where

$$D = (1 - \phi + \phi\zeta_2)\left[Z_1^s - (1 - \phi)Z_1^a \zeta_1\right]\tan(\delta_2 h) + (1 - \phi + \phi\zeta_1)\left[Z_2^a \zeta_2 (1 - \phi) - Z_2^s\right]\tan(\delta_1 h) \tag{3.16}$$

$$Z_1^a(\omega) = \left(C_3 + \frac{C_2}{\zeta_1}\right)\frac{\delta_1}{\phi\omega} Z_2^a(\omega) = \left(C_3 + \frac{C_2}{\zeta_2}\right)\frac{\delta_2}{\phi\omega} \tag{3.17}$$

$$Z_1^s(\omega) = (C_1 + C_2\zeta_1)\frac{\delta_1}{\omega} Z_2^s(\omega) = (C_1 + C_2\zeta_2)\frac{\delta_2}{\omega} \tag{3.18}$$

$$\zeta_1 = \frac{C_1\delta_1^2 - \omega^2\rho_{11}}{\omega^2\rho_{12} - C_2\delta_1^2}\zeta_2 = \frac{C_1\delta_2^2 - \omega^2\rho_{11}}{\omega^2\rho_{12} - C_2\delta_2^2} \tag{3.19}$$

$$\delta_1^2 = \frac{\omega^2}{2(C_1C_3 - C_2^2)}\left[C_1\rho_{22} + C_3\rho_{11} - 2C_2\rho_{12} - \sqrt{\Delta}\right] \tag{3.20a}$$

$$\delta_2^2 = \frac{\omega^2}{2(C_1C_3 - C_2^2)}\left[C_1\rho_{22} + C_3\rho_{11} - 2C_2\rho_{12} + \sqrt{\Delta}\right] \tag{3.20b}$$

$$\Delta = \left(C_1\rho_{22} + C_3\rho_{11} - 2C_2\rho_{12}\right)^2 - 4\left(C_1C_3 - C_2^2\right)\left(\rho_{11}\rho_{22} - \rho_{12}^2\right) \tag{3.21}$$

$$\rho_{11} = \rho_s + \rho_c - \frac{1}{\omega}j\sigma\phi^2\sqrt{1 + \frac{4j\alpha_\infty^2\eta\rho_0\omega}{\sigma^2\Lambda^2\phi^2}} \tag{3.22a}$$

$$\rho_{12} = -\rho_c + \frac{1}{\omega}j\sigma\phi^2\sqrt{1 + \frac{4j\alpha_\infty^2\eta\rho_0\omega}{\sigma^2\Lambda^2\phi^2}} \tag{3.22b}$$

$$\rho_{22} = \phi\rho_0 + \rho_c - \frac{1}{\omega}j\sigma\phi^2\sqrt{1 + \frac{4j\alpha_\infty^2\eta\rho_0\omega}{\sigma^2\Lambda^2\phi^2}} \tag{3.22c}$$

$$\rho_c = \phi\rho_0(\alpha_\infty - 1) \tag{3.23}$$

$$C_1 = \frac{4}{3}G_s + K_s + \frac{(1-\phi)^2}{\phi}KC_2 = (1-\phi)KC_3 = \phi K \tag{3.24}$$

$$G_s = \frac{E_s(1 + j\eta_s)}{2(1+\nu_s)}K_s = \frac{2G_s(1+\nu_s)}{3(1-2\nu_s)} \tag{3.25}$$

Here, δ_1 and δ_2 are the wave numbers of the compressional frame-borne and air-borne waves, ζ_1 and ζ_2 are the ratios of the velocities for the two compressional waves, and Z_1^a and Z_2^a and Z_1^s and Z_2^s are the characteristic impedances corresponding to transmission in air and frame, respectively (Allard and Atalla, 2009). The air bulk modulus$K$ is the same with the one for the Johnson-Champoux-Allard-Lafarge model given in Eq. (14).

3.1.6. Calculation of the physical parameters

There is a need to calculate the flow resistivity of the sample to calculate its SACs using the Delany-Bazley model. In addition to flow resistivity, it is necessary to determine the viscous and thermal characteristic lengths and the tortuosity of the porous sample to calculate its SACs using the Johnson-Champoux-Allard model. Furthermore, in addition to all the mentioned parameters above, the thermal static permeability is needed to calculate the SACs of a porous sample using the Johnson-Champoux-Allard-Lafarge and Biot-Allard models. Now, let's present some models for the estimation of these parameters. It should be noted that there are different models to predict flow resistivity (Cox and D'Antonio 2004; Mechel 2008). For example, for random fiber orientation, flow resistivity can be estimated using:

$$\sigma = 4\frac{\eta}{r_f^2}\left[0.55\frac{(1-\phi)^{4/3}}{\phi} + \sqrt{2}\frac{(1-\phi)^2}{\phi^3}\right] \tag{3.26}$$

where r_f is the fiber radius. Please note that the air viscosity is around $\eta = 1.82 \times 10^{-5}\,\mathrm{kgm^{-1}s^{-1}}$ at 20 °C and 101.3 kPa. Similarly, the other air parameters needed in calculation of the SACs of a porous

sample are $c_p = 1002$ J/kg/K, $\gamma = 1.4$, $P_r = 0.71$ and $\kappa = 0.026$ W/m/K at 20 °C and 101.3 kPa. The porosity ϕ can be predicted using:

$$\phi = 1 - \frac{\rho_s}{\rho_f} \tag{3.27}$$

where ρ_f is the fiber density, and ρ_s is the bulk or sample density. The tortuosity of porous samples can be estimated using (Bansod, Mittal, and Mohanty 2016):

$$\alpha_\infty = 1 + \frac{1-\phi}{2\phi} \tag{3.28}$$

The viscous and thermal characteristic lengths of the porous sample can be calculated using (Allard and Champoux 1992; Kino 2015):

$$\Lambda = \frac{1}{2\pi r_f l} \tag{3.29}$$

$$\Lambda' = \frac{1}{\pi r_f l} \tag{3.30}$$

where l is the total length of the fiber per unit volume given by:

$$l = \frac{1}{\pi r_f^2 \rho_f / \rho_s} \tag{3.31}$$

The static thermal permeability based on cylindrical pores assumption can be estimated using (Lafarge et al. 1997):

$$q_0' = \frac{\eta}{\sigma} \tag{3.32}$$

3.1.7. Evaluation of the models

The aforementioned mathematical models for the prediction of the SACs of porous samples are evaluated here. For this purpose, first, the SACs of a natural fiber sample are calculated using the models mentioned above, and the results are compared in Figure 6. The properties of this porous sample made from natural hemp fibers are $h = 40$ mm, $\phi = 0.93$, $\sigma = 4920$ Ns/m^4, $\alpha_\infty = 1.05$, $\wedge = 115$ μm, $\wedge' = 170$ μm, and $\rho_s = 88$ kg/m^3 (Santoni et al. 2019). Using Eq. (3.32), the thermal static permeability for this sample is calculated to be 3.7×10^{-9} m^2. Here, the shear modulus of the frame is assumed to be $G_s = 200000\,(1 + 0.1\,j)$ Pa. It is seen that the SACs predicted by the Johnson-Champoux-Allard, the Johnson-Champoux-Allard-Lafarge and Biot-Allard models are close to each other, and they are close to the experimental results. However, there are some differences between the results predicted by the Delany-Bazley (or Delany-Bazley-Miki) model and the experimental results. The small peak related to the frame resonance seen in the experimental curve between 750 and 850 Hz is successfully predicted by the Biot-Allard model. However, as can be seen, the effect of the frame resonance on the SACs of the porous sample is negligible. Another point is that, although the Delany-Bazley model produces negative SACs at low frequencies (i.e. f < 100 Hz), there is no negative value produced by the Delany-Bazley-Miki model.

The regression constants in the Delany-Bazley model can be tuned to match experimental results and predictions for specific frequency ranges and different porous samples. Unlike the Delany-Bazley model or its modified versions, the Johnson-Champoux-Allard and Johnson-Champoux-Allard-Lafarge models can predict some local maxima and minima seen in the experimental SAC curves. Furthermore, the Johnson-Champoux-Allard-Lafarge model can produce more accurate SACs at low frequencies, because static thermal permeability is used to describe the low-frequency behavior of

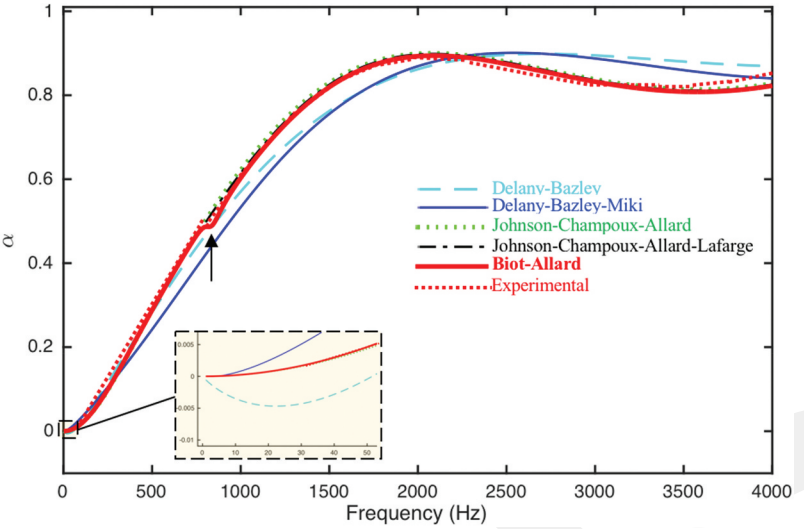

Figure 6. The SACs of a porous sample made from natural hemp fibers ($h = 40$ mm, $\phi = 0.93$, $\sigma = 4920$ Ns/m^4, $\alpha_\infty = 1.05$, $\wedge = 115$ μm, $\wedge' = 170$ μm, and $\rho_b = 88$ kg/m^3). Experimental data: (Santoni et al. 2019).

thermal effects in this model (Lafarge et al. 1997). Unlike all the models mentioned above, the Biot-Allard model can predict frame resonances. It should be noted that, for many porous materials including natural fiber samples excited by an incident acoustic wave, it is possible to assume that their frames are rigid, either due to the high value of the elastic modulus, or the high density, or because of special test conditions (Raj, Fatima, and Tandon 2020; Santoni et al. 2019). Therefore, the Johnson-Champoux-Allard and Johnson-Champoux-Allard-Lafarge models can produce the same SACs as the Biot-Allard model when the flow resistivity is not too high and the shear modulus of the frame is not too low (Moussatov, Ayrault, and Castagnede 2001; Wang, Kuo, and Chen 2008).

3.2. Prediction of sound transmission losses (STLs)

A typical STL curve is shown in Figure 7. There are specific material properties that dominate each frequency region. The stiffness of the sample determines the first frequency region that is between 0 and natural frequency (ω_{ij}). The behavior of the curve is determined by the mass of the sample in frequency range between natural and critical frequencies (ω_{ij} and ω_c). The part of the STL curve above the critical frequency is called the coincidence region, and the damping of the sample dominates this region. Based on these boundaries, the STLs of a sample is estimated using (Tadeu and Mateus 2001; Wang et al. 2011):

$$\mathrm{STL}(\omega) = 10\log\left\{\left(\frac{\bar{\rho}\omega}{2\rho_0 c_0}\right)^2\left[1-\left(\frac{\omega_{ij}}{\omega}\right)^2\right]^2\right\} 0 < \omega < \omega_{ij} \tag{3.33a}$$

$$\mathrm{STL}(\omega) = 10\log\left[1+\left(\frac{\bar{\rho}\omega}{2\rho_0 c_0}\right)^2\right] \omega_{ij} < \omega < \omega_c \tag{3.33b}$$

$$\mathrm{STL}(\omega) = 20\log\left(\frac{\bar{\rho}\omega}{2\rho_0 c_0}\right) + 10\log\left(\frac{2\eta\omega}{\pi\omega_c}\right) \omega_c < \omega \tag{3.33c}$$

where $\bar{\rho}$ is the sample surface density.

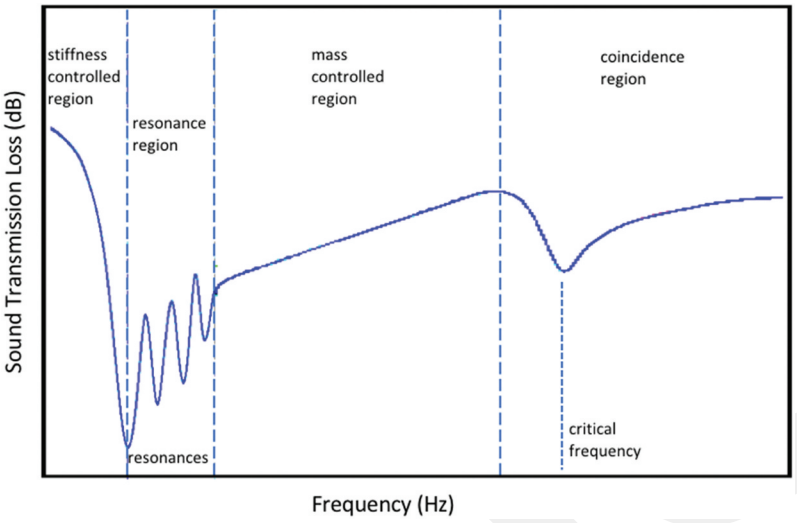

Figure 7. A typical STL curve.

Although the STLs of a sample can be estimated using the Johnson–Allard equivalent fluid model based on the transfer matrix, boundary and finite element methods (Alhijazi et al. 2020; Bansod, Mittal, and Mohanty 2016), the models presented here are very practical for the estimation of the STLs of structures, and to evaluate the measured results. In addition to the sample surface density $\bar{\rho}$, there is a need to determine the natural and critical frequencies of the sample to use these models. The natural frequency of a sample is given by:

$$\omega_{ij} = \frac{\lambda_{ij}^2}{a^2}\sqrt{\frac{E_s h^3}{12\rho_s h\left(1-\nu_s^2\right)}} \tag{3.34}$$

where a, h, ρ_s, E_s, and ν_s are the diameter, thickness, density, Young's modulus, and Poisson's ratio of the sample, respectively. Here, i and j are the nodal diameters and circles of the modes, whereas λ_{ij}^2 are the modal constants. For example, the modal constants are 10.22 and 39.77 for the modes (0,1) and (0,2), respectively, for a clamped circle sample (Dragonetti et al. 2020). The critical frequency of a sample can be determined using (Norton and Karczub 2003):

$$\omega_c = c_0^2\sqrt{\frac{12\rho_s\left(1-\nu_s^2\right)}{E_s h^3}} \tag{3.35}$$

4. Acoustic properties

The SACs at different frequencies and NRCs for many natural fibers are presented here. Unlike some review studies in the literature, not only the SACs and thicknesses of the samples are presented, but also their bulk densities and flow resistivities are included in the tables here. In addition, the SACs of the samples are normalized using their bulk density and thickness, hence the sound absorption performance of the samples per unit mass is presented. Based on the normalized results of many natural fiber samples, an empirical model for the estimation of the SACs of porous samples is presented. Although there are various studies on the SACs of natural fiber samples, limited number of studies included the STLs of these materials, therefore the STLs of some natural fiber samples are presented in this section.

4.1. Sound absorption coefficients (SACs)

The SACs and NRCs of common natural fiber samples, including coconut, cotton, flax, hemp, jute, kapok, kenaf, ramie and sisal are listed in Table 4. Since the SACs of porous samples are strongly dependent on the bulk density, thickness and flow resistivity of the samples, they are clearly indicated in Table 4. In addition, the diameter and density of the fibers are included in Table 4. For comparison purposes, in addition to the SACs of the natural fiber samples, the SACs of the natural jute felt and wool, synthetic polyester fiber and glass wool samples are listed in Table 4. It is seen that the SACs of many natural fiber samples, such as cotton, flax, jute, kapok and ramie can be higher than those of glass wool samples of the same thickness. Almost all natural fiber samples given here have better sound absorption performance than polyester fiber samples of the same thickness.

The NRCs of various natural fiber samples with a thickness of 40 mm are plotted in Figure 8a. It is seen that the SACs of the jute and flax fiber samples are higher than those of the other samples. However, it should be noted that, although the thicknesses of these samples are the same, their bulk densities (masses) are quite different. In order to obtain a parameter that reflects the effect of the specimen mass, the NRC of the sample is divided by its thickness (h) and bulk density (ρ_s):

$$\mathrm{NRC}' = \frac{\mathrm{NRC}}{h\rho_s} \tag{4.1}$$

The results obtained using this new normalized parameter for the natural fiber samples in Figure 8a are plotted in Figure 8b. It is clearly seen that the coconut, date palm, hemp, kenaf, and sisal fiber samples have higher sound absorption per unit mass than the flax, jute and ramie fiber samples. The results clearly show that the sound absorption performance per unit mass for the kapok sample is very high compared to the other samples. Similarly, the SACs can be normalized using h and ρ_s:

$$\mathrm{SAC}' = \frac{\mathrm{SAC}}{h\rho_s} \tag{4.2}$$

The normalized SACs and NRCs for all the samples in Table 4 are calculated and listed in Table 5. The results show that, for some natural fiber samples, such as hemp and kapok, the sound absorption performance per unit mass can be higher than that of polyester fiber and glass wool samples.

The NRCs and normalized NRCs of the natural fiber samples in Figure 8 are plotted in Figure 9 as a function of the bulk density. It is seen that there is no correlation between NRC and bulk density (Figure 9a). However, there is a strong correlation between the normalized NRC (or NRC′) and bulk density (i.e. $R^2 = 0.97$) as seen in Figure 9b.

Now, the normalized NRCs and SACs for different frequencies are plotted as a function of the bulk density for all natural fiber samples with different thicknesses in Table 4 to see whether there is a relationship between the normalized parameters and the bulk density. Overall, the normalized SACs for 500, 1000 and 2000 Hz and the normalized NRCs are plotted in Figure 10. It is seen that there is a good correlation between the normalized SAC and the bulk density for 500, 1000 and 2000 Hz ($R^2 > 0.8$), and a perfect correlation between the normalized NRC and the bulk density ($R^2 = 0.92$) for different natural fiber samples with different thickness and flow resistivity values. The relationship between the normalized NRC and bulk density is given by $A\rho_s^{-\tau}$. Hence, the following expression can be written:

$$\alpha' = \frac{\alpha}{h\rho_s} = A\rho_s^{-\tau} \tag{4.3}$$

Thus, we can write the following empirical model for the estimation of the SACs of porous samples:

$$\alpha = Ah\rho_s^{(1-\tau)} \tag{4.4}$$

Table 4. The bulk densities, thicknesses, flow resistivities, SACs and NRCs for natural fiber samples, natural jute felt and wool, synthetic polyester fiber and glass wool samples.

Natural Fiber	Bulk Density (kg/m^3)	Thickness (mm)	Fiber Diameter (μm)	Fiber Density (kg/m^3)	Flow Resistivity ($Pa\ s/m^2$)	SAC Frequency (Hz) 125	250	500	1000	2000	NRC	Reference
Coconut Fiber	110	21	-	-	1187	0.12	0.15	0.16	0.22	0.51	0.26	Bhingare and Prakash 2020
	110	28	-	-	1093	0.17	0.19	0.20	0.28	0.67	0.34	
	110	35	-	-	1013	0.20	0.20	0.23	0.30	0.73	0.37	
	220	21	-	-	3483	0.15	0.18	0.19	0.25	0.55	0.29	
	220	28	-	-	3265	0.19	0.19	0.20	0.28	0.71	0.35	
	220	35	-	-	3152	0.22	0.23	0.24	0.34	0.79	0.40	
	130	25	263	541	4810	0.02	0.03	0.05	0.10	0.45	0.16	Taban et al. 2019c
	130	35			4680	0.07	0.10	0.11	0.33	0.90	0.36	
	130	45			4535	0.05	0.13	0.28	0.90	0.72	0.51	
	60	50	250	-	1500	0.10	0.20	0.34	0.67	0.79	0.50	Berardi and Iannace 2015
Cotton Fiber	41	50	14	1530	22342	0.06	0.16	0.50	0.95	0.92	0.63	Oldham, Egan, and Cookson 2011
Date Palm Fiber	100	10	465	930	1940	0.01	0.05	0.08	0.17	0.42	0.18	Taban et al. 2019a
	100	20			1785	0.03	0.08	0.10	0.18	0.68	0.26	
	100	30			1673	0.03	0.09	0.13	0.38	0.78	0.35	
	100	40			1535	0.05	0.13	0.23	0.55	0.83	0.44	
	200	10			5910	0.02	0.06	0.09	0.23	0.48	0.22	
	200	20			5768	0.03	0.07	0.09	0.28	0.80	0.31	
	200	30			5580	0.04	0.09	0.17	0.42	0.82	0.38	
	200	40			5470	0.06	0.10	0.25	0.58	0.86	0.45	
	65	20	420	930	1068	0.02	0.06	0.10	0.16	0.65	0.24	Taban et al. 2019b
	65	30			956	0.03	0.08	0.15	0.38	0.79	0.35	
	65	40			879	0.05	0.10	0.22	0.52	0.84	0.42	
Esparto Grass Fiber	101	30	-	-	2980	0.14	0.15	0.18	0.40	0.78	0.38	Arenas et al. 2020
	104	49	-	-	2980	0.21	0.21	0.25	0.68	0.83	0.49	
Flax Fiber	78	50	22	1500	20393	0.07	0.20	0.50	0.90	0.98	0.65	Oldham, Egan, and Cookson 2011
	341	40	15		83421	0.22	0.31	0.52	0.81	0.80	0.65	Yang and Yan 2012
Hemp Fiber	50	30	-	-	1400	0.01	0.15	0.25	0.51	0.70	0.40	Berardi and Iannace 2015
	88	40	27	1300	5536	0.05	0.10	0.24	0.63	0.83	0.45	Santoni et al. 2019
Jute Fiber	66	50	81	1370	1497	0.06	0.12	0.25	0.65	0.80	0.46	Oldham, Egan, and Cookson 2011
	411	40	58		19790	0.20	0.26	0.48	0.88	0.93	0.65	Yang and Yan 2012
	445	25	68	1084	20087	0.06	0.16	0.27	0.63	0.97	0.40	Bansod, Mittal, and Mohanty 2016
	445	50			20087	0.10	0.29	0.77	0.95	0.85	0.60	
Kapok Fiber	25	60	15–23	370	42046	0.22	0.37	0.54	0.83	0.93	0.67	Xiang et al. 2013
	42	60			97944	0.24	0.30	0.64	0.66	0.86	0.61	
	58	60			165755	0.19	0.24	0.30	0.52	0.73	0.45	
	15	17			18286	0.03	0.06	0.11	0.38	0.70	0.31	
	15	20			18286	0.07	0.09	0.16	0.41	0.79	0.36	
	15	40			18286	0.11	0.14	0.40	0.86	0.98	0.60	
	20	20			29225	0.07	0.09	0.19	0.55	0.89	0.43	
	20	40			29225	0.11	0.20	0.44	0.91	0.95	0.62	

(*Continued*)

Table 4. (Continued).

Natural Fiber	Bulk Density (kg/m^3)	Thickness (mm)	Fiber Diameter (μm)	Fiber Density (kg/m^3)	Flow Resistivity (Pa s/m^2)	SAC Frequency (Hz) 125	250	500	1000	2000	NRC	Reference
Kenaf	50	60	-	-	2700	0.09	0.19	0.33	0.68	0.90	0.55	Berardi and
Fiber	100	40	-	-	3500	0.08	0.18	0.32	0.70	0.94	0.55	Iannace
	100	60	-	-	3500	0.10	0.30	0.61	0.99	0.95	0.70	2015
	150	10	81	1400	4150	0.03	0.05	0.04	0.10	0.20	0.10	Taban et al.
	150	20			3620	0.05	0.07	0.10	0.28	0.70	0.29	2020
	150	30			3620	0.08	0.10	0.18	0.55	0.95	0.45	
	150	40			3230	0.10	0.12	0.24	0.70	0.88	0.49	
	200	10			6940	0.03	0.05	0.08	0.13	0.43	0.17	
	200	20			6910	0.04	0.06	0.23	0.41	0.97	0.42	
	200	30			5680	0.05	0.10	0.20	0.75	0.90	0.49	
	200	40			5470	0.06	0.12	0.34	0.98	0.83	0.57	
Oil Palm Fiber	227	50	-	-	18823	0.04	0.10	0.24	0.74	0.78	0.47	Sambu et al. 2016
Ramie Fiber	96	50	24	1500	24465	0.08	0.22	0.65	0.88	0.92	0.67	Oldham, Egan, and Cookson 2011
	443	40			123782	0.15	0.25	0.55	0.63	0.70	0.60	Yang and Yan 2012
Sisal Fiber	215	44	202	-	4180	0.10	0.12	0.26	0.74	0.97	0.52	Da Silva et al. 2019
Natural Felt and Wool												
Jute Felt	242	25	68	1084	33190	0.08	0.08	0.26	0.56	0.94	0.50	Bansod, Mittal,
	242	50			33190	0.22	0.33	0.63	0.96	0.92	0.70	and Mohanty 2016
	148	10	33		28852	0.05	0.09	0.26	0.60	0.87	0.46	Bansod and Mohanty 2016
Sheep Wool	20	50	37	1300	1570	0.07	0.12	0.22	0.43	0.60	0.34	Oldham, Egan, and Cookson 2011
	40	40	-	-	2100	0.10	0.14	0.36	0.73	0.94	0.55	Berardi and
	40	60	-	-	2100	0.15	0.28	0.66	0.95	0.94	0.70	Iannace 2015
Synthetic Fiber and Wool												
Glass	20	54	7	2550	6600	0.07	0.18	0.48	0.82	0.94	0.61	Komatsu 2008;
Wool	91	27			53100	0.04	0.08	0.37	0.77	0.93	0.54	Tarnow 2002
Polyester	30	20	18–48	-	2986	0.03	0.07	0.10	0.16	0.28	0.15	Garai and
Fiber	40	40		-	5112	0.10	0.13	0.27	0.52	0.79	0.43	Pompoli 2005

The values of A and τ determined for the SACs at different frequencies and NRC are listed in Table 6. Requiring only the bulk density and thickness of the sample, this simple empirical model can be used for rough estimation of the SACs of a porous sample, and to evaluate the measured results.

4.2 Sound transmission losses (STLs)

The STLs of some porous natural fiber samples as well as their averages are listed in Table 7. As expected, it is seen that STL increases as the bulk density and thickness of the sample increases. The STLs of some natural fiber samples with a thickness of 30 mm are plotted in Figure 11. It is seen that the natural fiber samples have low STLs. The low STLs of natural fiber samples are due to their high porosity and low density. On the other hand, the STLs of some natural fiber samples such as jute are higher than those of the acoustic foams such as polypropylene. Overall, in addition to the sound

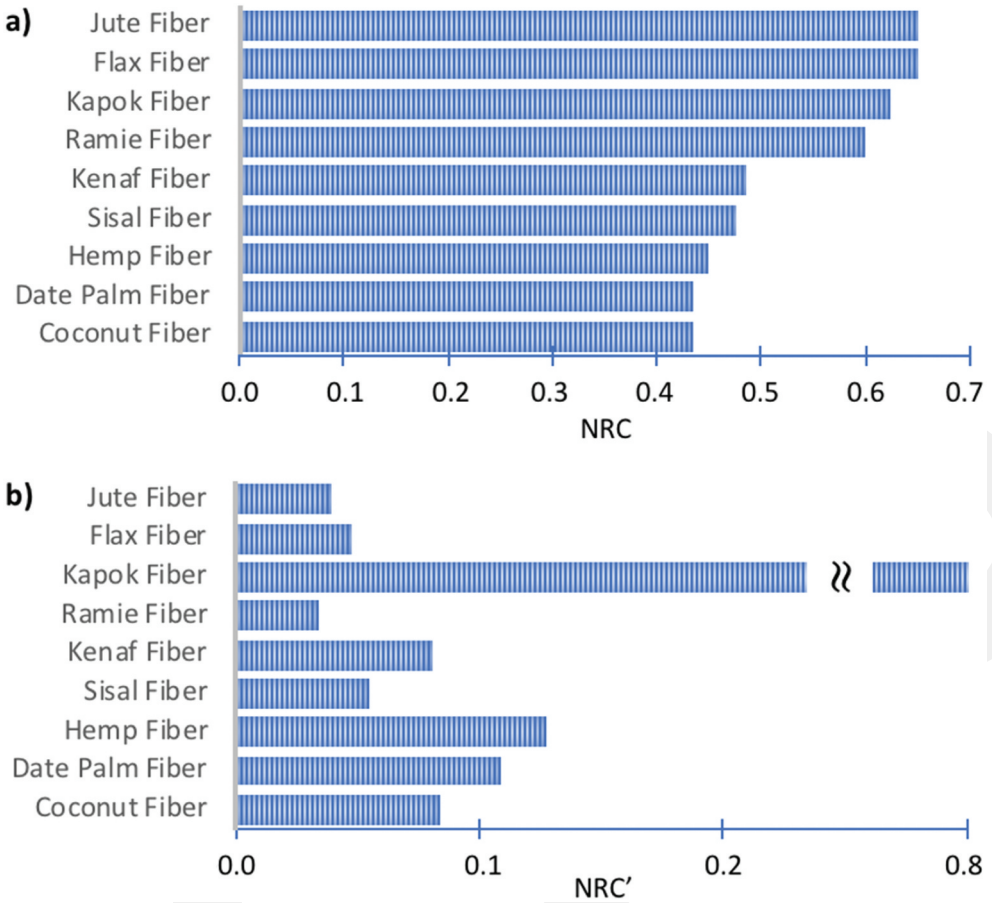

Figure 8. The sound absorption performances of different natural fiber samples with a thickness of 40 mm: (a) NRC and (b) normalized NRC.

absorption provided by natural fiber structures, their insulation capability can provide a considerable sound transmission loss in practical applications. It should be noted that there are only a few studies on the STLs of natural fiber samples, so it seems that more research is needed on the STLs of natural fiber samples. For the desired values of the SACs and STLs of a porous sample, the bulk density, thickness, and flow resistivity of the sample need to be optimized.

5. Concluding remarks

A critical assessment of the acoustic properties of natural fiber samples was performed in this paper. The contributions of this study are summarized as follows. The common techniques for both the measurement and prediction of the SACs and STLs of natural fiber samples were determined, presented, and evaluated. The SACs of many natural fibers, including coconut, cotton, flax, hemp, jute, ramie and sisal fibers, which are the world's major plant fibers, were presented along with the thickness, bulk density and flow resistivity of the samples. The SACs of the samples were normalized using their thickness and bulk density, and the sound absorption performance of the samples per unit mass was presented. Based on the normalized results of many natural fiber samples, an empirical model for the estimation of the SACs of porous samples was presented. The STLs of some natural fiber samples were presented.

Table 5. The normalized SACs and NRCs for all the samples in Table 4.

Natural Fiber	Bulk Density (kg/m^3)	Thickness (mm)	SAC' Frequency (Hz) 125	250	500	1000	2000	NRC'	Reference
Coconut Fiber	110	21	0.05	0.06	0.07	0.10	0.22	0.11	Bhingare and Prakash 2020
	110	28	0.06	0.06	0.06	0.09	0.22	0.11	
	110	35	0.05	0.05	0.06	0.08	0.19	0.09	
	220	21	0.03	0.04	0.04	0.05	0.12	0.06	
	220	28	0.03	0.03	0.03	0.05	0.12	0.06	
	220	35	0.03	0.03	0.03	0.04	0.10	0.05	
	130	25	0.01	0.01	0.02	0.03	0.14	0.05	Taban et al. 2019c
	130	35	0.02	0.02	0.02	0.07	0.20	0.08	
	130	45	0.01	0.02	0.05	0.15	0.12	0.09	
	60	50	0.03	0.07	0.11	0.22	0.26	0.17	Berardi and Iannace 2015
Cotton Fiber	41	50	0.03	0.08	0.25	0.47	0.45	0.31	Oldham, Egan, and Cookson 2011
Date Palm Fiber	100	10	0.01	0.05	0.08	0.17	0.42	0.18	Taban et al. 2019a
	100	20	0.02	0.04	0.05	0.09	0.34	0.13	
	100	30	0.01	0.03	0.04	0.13	0.26	0.12	
	100	40	0.01	0.03	0.06	0.14	0.21	0.11	
	200	10	0.01	0.03	0.05	0.12	0.24	0.11	
	200	20	0.01	0.02	0.02	0.07	0.20	0.08	
	200	30	0.01	0.02	0.03	0.07	0.14	0.06	
	200	40	0.01	0.01	0.03	0.07	0.11	0.06	
	65	20	0.02	0.05	0.08	0.12	0.50	0.19	Taban et al. 2019b
	65	30	0.02	0.04	0.08	0.19	0.41	0.18	
	65	40	0.02	0.04	0.08	0.20	0.32	0.16	
Esparto Grass	101	30	0.05	0.05	0.06	0.13	0.26	0.13	Arenas et al. 2020
Fiber	104	49	0.04	0.04	0.05	0.13	0.16	0.10	
Flax Fiber	78	50	0.02	0.05	0.13	0.23	0.25	0.16	Oldham, Egan, and Cookson 2011
	341	40	0.02	0.02	0.04	0.06	0.06	0.05	Yang and Yan 2012
Hemp Fiber	50	30	0.01	0.10	0.17	0.34	0.47	0.27	Berardi and Iannace 2015
	88	40	0.01	0.03	0.07	0.18	0.24	0.13	Santoni et al. 2019
Jute Fiber	66	50	0.02	0.04	0.08	0.20	0.24	0.14	Oldham, Egan, and Cookson 2011
	411	40	0.01	0.02	0.03	0.05	0.06	0.04	Yang and Yan 2012
	445	25	0.01	0.01	0.02	0.06	0.09	0.04	Bansod, Mittal, and Mohanty 2016
	445	50	0.00	0.01	0.03	0.04	0.04	0.03	
Kapok Fiber	25	60	0.15	0.25	0.36	0.55	0.62	0.45	Xiang et al. 2013
	42	60	0.09	0.12	0.25	0.26	0.34	0.24	
	58	60	0.05	0.07	0.09	0.15	0.21	0.13	
	15	17	0.11	0.23	0.42	1.46	2.68	1.20	
	15	20	0.22	0.30	0.53	1.38	2.62	1.21	
	15	40	0.18	0.24	0.66	1.44	1.64	1.00	
	20	20	0.18	0.24	0.46	1.37	2.23	1.08	
	20	40	0.14	0.26	0.55	1.13	1.18	0.78	
Kenaf Fiber	50	60	0.03	0.06	0.11	0.23	0.30	0.18	Berardi and Iannace 2015
	100	40	0.02	0.05	0.08	0.18	0.24	0.14	
	100	60	0.02	0.05	0.10	0.17	0.16	0.12	
	150	10	0.02	0.03	0.03	0.07	0.13	0.07	Taban et al. 2020
	150	20	0.02	0.02	0.03	0.09	0.23	0.10	
	150	30	0.02	0.02	0.04	0.12	0.21	0.10	
	150	40	0.02	0.02	0.04	0.12	0.15	0.08	
	200	10	0.02	0.03	0.04	0.07	0.22	0.09	
	200	20	0.01	0.02	0.06	0.10	0.24	0.10	
	200	30	0.01	0.02	0.03	0.13	0.15	0.08	
	200	40	0.01	0.02	0.04	0.12	0.10	0.07	
Oil Palm Fiber	227	50	0.00	0.01	0.02	0.07	0.07	0.04	Sambu et al. 2016
Ramie Fiber	96	50	0.02	0.05	0.14	0.18	0.19	0.14	Oldham, Egan, and Cookson 2011
	443	40	0.01	0.01	0.03	0.04	0.04	0.03	Yang and Yan 2012
Sisal Fiber	215	44	0.01	0.01	0.03	0.08	0.10	0.05	Da Silva et al. 2019
Natural Felt and Wool									

(*Continued*)

Table 5. (Continued).

Natural Fiber	Bulk Density (kg/m^3)	Thickness (mm)	SAC′ Frequency (Hz) 125	250	500	1000	2000	NRC′	Reference
Jute Felt	242	25	0.01	0.01	0.04	0.09	0.16	0.08	Bansod, Mittal, and Mohanty 2016
	242	50	0.02	0.03	0.05	0.08	0.08	0.06	
	148	10	0.03	0.06	0.18	0.40	0.59	0.31	Bansod and Mohanty 2016
Sheep Wool	20	50	0.07	0.12	0.22	0.43	0.61	0.35	Oldham, Egan, and Cookson 2011
	40	40	0.06	0.09	0.23	0.46	0.59	0.34	Berardi and Iannace 2015
	40	60	0.06	0.12	0.28	0.40	0.39	0.29	
Synthetic Fiber and Wool									
Glass Wool	20	54	0.06	0.17	0.44	0.76	0.87	0.56	Komatsu 2008; Tarnow 2002
	91	27	0.02	0.03	0.15	0.32	0.39	0.22	
Polyester Fiber	30	20	0.05	0.12	0.17	0.27	0.47	0.25	Garai and Pompoli 2005
	40	40	0.06	0.08	0.17	0.33	0.49	0.27	

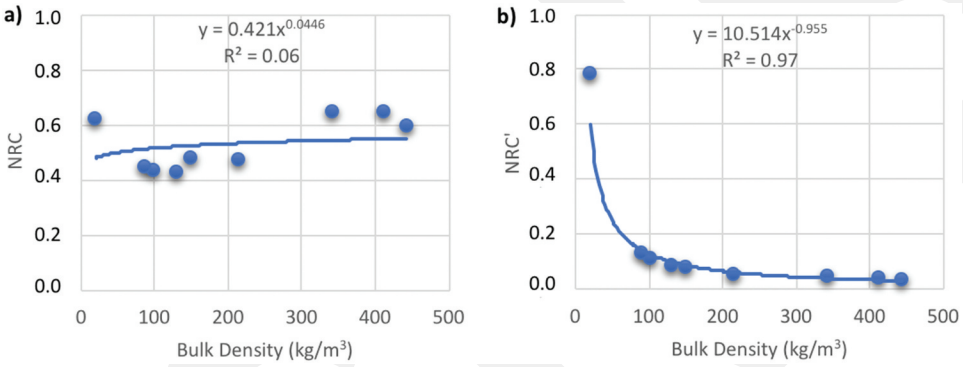

Figure 9. The sound absorption performances of samples of different natural fiber samples with a thickness of 40 mm as a function of the bulk density: (a) NRC and (b) normalized NRC.

- The two-microphone transfer function method is commonly used in practice, and there are several studies on the use of the reverberation room method to determine the SACs of natural fiber samples. It is worth remembering that the two-microphone transfer function method is delineated in the ISO 10534–2 and ASTM E1050 standards, and the reverberation room method is described in the ISO 354 and ASTM C423 standards.
- The four-microphone transfer matrix method is commonly used in practice, while there are a few studies on the use of the conventional two-room method to determine the STLs of natural fiber samples. It is noted that the four-microphone transfer matrix method is delineated in the ASTM E2611, and the conventional two-room method is explained in the ASTM E90 standard.
- Although they require small test samples, and they are quite practical, only normal-incidence SACs and STLs in a limited frequency range that is imposed by tube dimensions can be measured with impedance tube tests, and the mounting condition of the test sample in the tubes can affect the SACs and STLs measured in impedance tube tests. On the other hand, the random-incidence SACs and STLs with limited edge effect for a wide frequency range can be measured via the reverberation room and two-room methods. The advantages and limitations of these methods are summarized in Section 2.3 and Figure 5.
- The Delany-Bazley and Johnson–Champoux–Allard models are widely used to predict the acoustic properties of natural fiber samples. There is a need to calculate the flow resistivity of the sample to calculate its SACs using the Delany-Bazley model. In addition to the flow resistivity, it is necessary to determine the viscous and thermal characteristic lengths and the

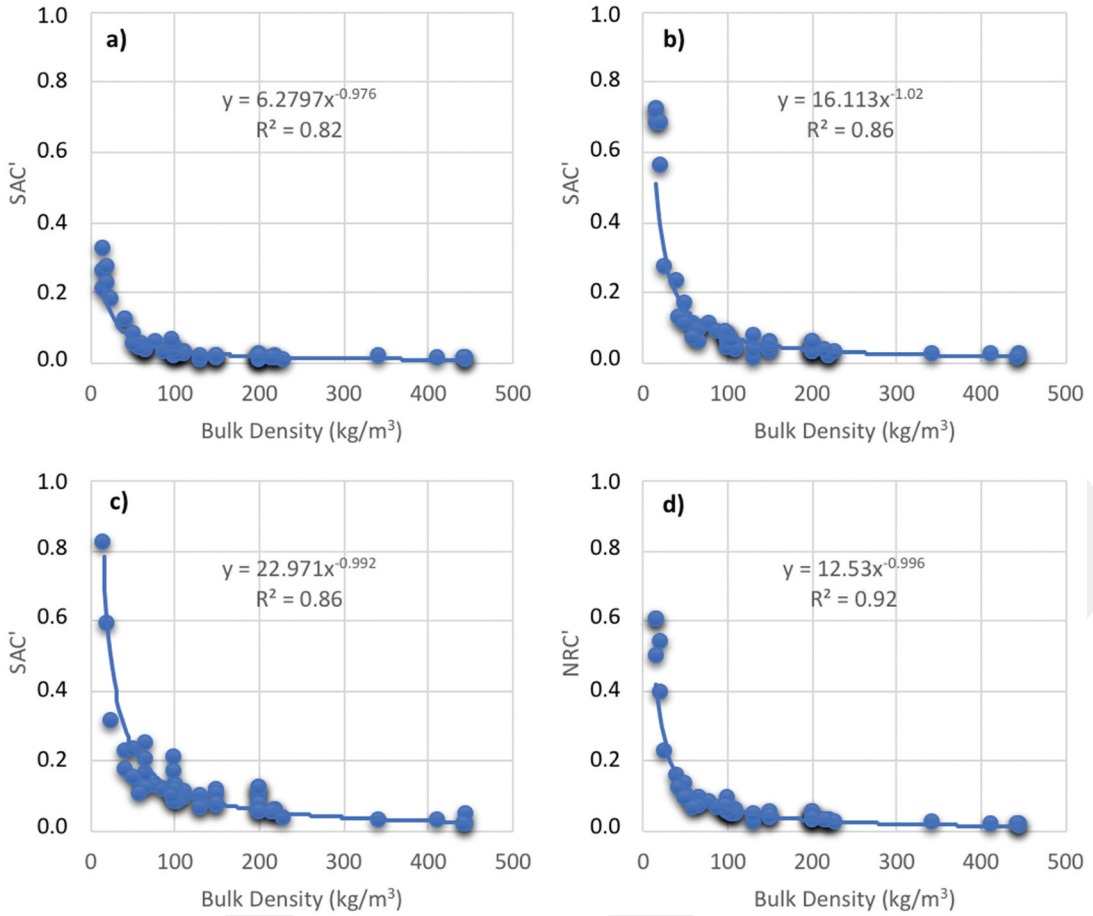

Figure 10. The normalized SACs for (a) 500, (b) 1000 and (c) 2000 Hz and (d) normalized NRCs.

Table 6. The values of A and τ for the model $\alpha = A h \rho_s^{(1-\tau)}$.

Frequency (Hz)	A	τ
125	1.3083	0.893
250	2.9933	0.936
500	6.2797	0.976
1000	16.113	1.020
2000	22.971	0.992
NRC	12.530	0.996

tortuosity of the porous sample to calculate its SACs using the Johnson-Champoux-Allard model. In addition to all the parameters mentioned above, thermal static permeability is required to calculate the SACs of a porous sample using the Johnson-Champoux-Allard-Lafarge and Biot-Allard models. The Johnson-Champoux-Allard and Johnson-Champoux-Allard-Lafarge rigid-frame models can predict not only the general trend, but also local maxima and minima seen in the experimental SAC curves. Furthermore, the Biot-Allard deformable-frame model can predict frame resonances. All these models are compared and evaluated in Section 3.1.7.

Table 7. The STLs of some natural fiber samples and polypropylene foam.

Sample	Bulk Density (kg/m^3)	Thickness (mm)	Flow Resistivity (Pa s/m^2)	STL (dB) Frequency (Hz) 125	250	500	1000	2000	Ave	Reference
Banana Fiber	144	30	-	0.6	0.2	0.5	0.4	3.0	1.0	Kesharwani, Bedi, and Bahl 2020
Coconut Fiber	111	30	-	0.4	0.6	0.9	0.8	0.8	0.8	Kesharwani, Bedi, and Bahl 2020
	220	28	3265	3.1	3.2	3.7	3.0	9.0	4.7	Bhingare and Prakash 2020
	220	35	3152	3.5	3.4	3.0	3.8	9.2	4.9	
Cotton Fiber	18	35	-	1.1	1.1	1.6	2.5	3.0	2.1	Chen and Jiang 2009
Hemp Fiber	166	30	-	1.8	0.5	0.6	1.0	6.0	2.0	Kesharwani, Bedi, and Bahl 2020
Jute Fiber	129	30	-	3.3	1.4	1.5	2.8	9.6	3.8	
Jute Felt	242	25	33190	-	-	5.9	6.2	6.8	6.3	Bansod, Mittal, and Mohanty 2016
	242	50		-	-	8.7	9.7	11.7	10	
Kenaf Fiber	149	30	-	3.4	1.2	2.6	3.2	10.5	4.4	Kesharwani, Bedi, and Bahl 2020
Luffa Fiber	70	12	-	0.0	0.0	2.0	1.0	2.0	1.3	Koruk and Genc 2015
Ramie Fiber	51	35	-	1.7	1.6	1.9	2.8	3.3	2.4	Chen and Jiang 2009
Polypropylene Foam	67	35	-	1.1	1.0	1.2	1.8	2.2	1.6	

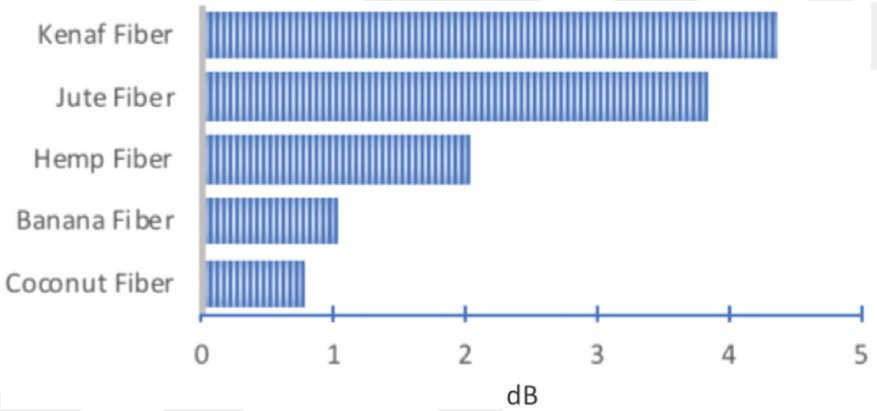

Figure 11. The STLs of some natural fiber samples with a thickness of 30 mm.

- Although the STLs of a sample can be estimated using the Johnson–Allard equivalent fluid model based on the transfer matrix, boundary and finite element methods, the basic models presented in Section 3.2 can be used for rough estimation of the STLs of samples, and to evaluate the experimental results. While the main input in these models is the sample surface density, it is necessary to calculate the natural and critical frequencies of the sample to use these models.
- Not only the SACs and NRCs for widely used natural fibers, including coconut, cotton, flax, hemp, jute, kapok, kenaf, ramie and sisal, but also the bulk density, thickness and flow resistivity of the samples are listed in Table 4. Furthermore, the SACs and NRCs of the samples are normalized using the thickness and bulk density of the samples to obtain a parameter for sound absorption reflecting the effect of mass, and the results are listed in Table 5. It is seen that the SACs of many natural fiber samples, such as cotton, flax, jute, kapok and ramie can be higher that the SACs of polyester fiber and glass wool samples of the same thickness. For some natural fiber samples, such as hemp and kapok, the sound absorption performance per unit mass can be higher than that of polyester fiber and glass wool samples.
- The results show that there is a good correlation between the normalized SAC and the bulk density for different frequencies, and a perfect correlation between the normalized NRC and the

bulk density for natural fiber samples with different thickness and flow resistivity values. Based on this correlation, an empirical model for the estimation of the SACs of porous samples is obtained. This model is given by SAC $= Ah\rho_s^{(1-\tau)}$ where A and τ are some constants (given in Table 6 for different frequencies), and h and ρ_s are the sample thickness and bulk density, respectively. This simple empirical model can be used for rough estimation of the SACs of a porous sample, and to evaluate the measured results.

- The results show that natural fiber samples have low STLs due to their high porosity and low density. On the other hand, the STLs of some natural fiber samples such as jute are higher than those of the acoustic foams such as polypropylene. However, it is observed that more research is needed on the STLs of natural fiber samples.

Acknowledgments

This work was supported by TUBITAK (The Scientific and Technological Research Council of Turkey) under Grant 119M115.

References

Alhijazi, M., Q. Zeeshan, Z. Qin, B. Safaei, and M. Asmael. 2020. Finite element analysis of natural fibers composites: A review. *Nanotechnology Reviews* 9 (1):853–75. doi:10.1515/ntrev-2020-0069.

Allard, J.-F., and N. Attala. 2009. *Propagation of sound in porous media: Modelling sound absorbing materials*. 2nd ed ed. Hoboken, NJ: Wiley & Sons Ltd.

Allard, J.-F., and Y. Champoux. 1992. New empirical equations for sound propagation in rigid frame fibrous materials. *The Journal of the Acoustical Society of America* 91 (6):3346–53. doi:10.1121/1.402824.

Arenas, J. P., R. Del Rey, J. Alba, and R. Oltra. 2020. Sound-absorption properties of materials made of esparto grass fibers. *Sustainability* 12 (14):5533. doi:10.3390/su12145533.

ASTM (American Society for Testing and Materials). 2016. ASTM E90-09(2016) Standard test method for laboratory measurement of airborne sound transmission loss of building partitions and elements.

ASTM (American Society for Testing and Materials). 2017. ASTM C423-17 Standard test method for sound absorption and sound absorption coefficients by the reverberation room method.

ASTM (American Society for Testing and Materials). 2019a. ASTM E1050-19 Standard test method for impedance and absorption of acoustical materials using a tube, two microphones and a digital frequency analysis system.

ASTM (American Society for Testing and Materials). 2019b. ASTM E2611-19 Standard test method for normal incidence determination of porous material acoustical properties based on the transfer matrix method.

Bansod, P. V., T. Mittal, and A. R. Mohanty. 2016. Study on the acoustical properties of natural jute material by theoretical and experimental methods for building acoustics applications. *Acoustics Australia* 47 (3):457–72. doi:10.1007/s40857-016-0073-4.

Bansod, P. V., and A. R. Mohanty. 2016. Inverse acoustical characterization of natural jute sound absorbing material by the particle swarm optimization method. *Applied Acoustics* 112:41–52. doi:10.1016/j.apacoust.2016.05.011.

Berardi, U., and G. Iannace. 2015. Acoustic characterization of natural fibers for sound absorption applications. *Building and Environment* 94:840–52. doi:10.1016/j.buildenv.2015.05.029.

Berardi, U., and G. Iannace. 2017. Predicting the sound absorption of natural materials: Best-fit inverse laws for the acoustic impedance and the propagation constant. *Applied Acoustics* 115:131–38. doi:10.1016/j.apacoust.2016.08.012.

Berardi, U., G. Iannace, and M. Di Gabriele. 2017. The acoustic characterization of broom fibers. *Journal of Natural Fibers* 14 (6):858–63. doi:10.1080/15440478.2017.1279995.

Bhingare, N. H., and S. Prakash. 2020. An experimental and theoretical investigation of coconut coir material for sound absorption characteristics. *Materials Today: Proceedings*. doi:10.1016/j.matpr.2020.09.401.

Bhingare, N. H., S. Prakash, and S. J. Vijaykumar. 2019. A review on natural and waste material composite as acoustic material. *Polymer Testing* 80:106142. doi:10.1016/j.polymertesting.2019.106142.

Bolton, J. S., T. Yoo, and O. Olivieri. 2007. *Measurement of normal incidence transmission loss and other acoustical properties of materials placed in a standing wave tube*. Denmark: Brüel & Kjær.

Champoux, Y., and J.-F. Allard. 1991. Dynamic tortuosity and bulk modulus in air-saturated porous media. *Journal of Applied Physics* 70 (4):1975–79. doi:10.1063/1.349482.

Chen, Y., and N. Jiang. 2009. Carbonized and activated non-woven as high performance acoustic materials: Part II noise insulation. *Textile Research Journal* 79 (3):213–18. doi:10.1177/0040517508093593.

Cox, T. J., and P. D'Antonio. 2004. *Acoustic absorbers and diffusers: Theory, design and application*. London, UK: Spon Press.

Da Silva, C. C. B., F. J. H. Terashima, N. Barbieri, and K. F. De Lima. 2019. Sound absorption coefficient assessment of sisal, coconut husk and sugar cane fibers for low frequencies based on three different methods. *Applied Acoustics* 156:92–100. doi:10.1016/j.apacoust.2019.07.001.

Das, O., R. E. Neisiany, A. J. Capezza, M. S. Hedenqvist, M. Försth, Q. Xu, L. Jiang, D. Ji, and S. Ramakrishna. 2020. The need for fully bio-based facemasks to counter coronavirus outbreaks: A perspective. *Science of the Total Environment* 736:139611. doi:10.1016/j.scitotenv.2020.139611.

Delany, M. E., and E. N. Bazley. 1970. Acoustical properties of fibrous absorbent materials. *Applied Acoustics* 3 (2):105–16. doi:10.1016/0003-682X(70)90031-9.

Dragonetti, R., M. Napolitano, L. Boccarusso, and M. Durante. 2020. A study on the sound transmission loss of a new lightweight hemp/bio-epoxy sandwich structure. *Applied Acoustics* 167:107379. doi:10.1016/j.apacoust.2020.107379.

Dunn, J. P., and W. A. Davern. 1986. Calculation of acoustic impedance of multi-layer absorbers. *Applied Acoustics* 19 (5):321–34. doi:10.1016/0003-682X(86)90044-7.

Fouladi, M. H., M. Ayub, and M. J. M. Nor. 2011. Analysis of coir fiber acoustical characteristics. *Applied Acoustics* 72 (1):35–42. doi:10.1016/j.apacoust.2010.09.007.

Garai, M., and F. Pompoli. 2005. A simple empirical model of polyester fibre materials for acoustical applications. *Applied Acoustics* 66 (12):1383–98. doi:10.1016/j.apacoust.2005.04.008.

Gokulkumar, S., P. R. Thyla, L. Prabhu, and S. Sathish. 2020. Measuring methods of acoustic properties and influence of physical parameters on natural fibers: A review. *Journal of Natural Fibers* 17 (12):1719–38. doi:10.1080/15440478.2019.1598913.

Gurunathan, T., S. Mohanty, and S. K. Nayak. 2015. A review of the recent developments in biocomposites based on natural fibres and their application perspectives. *Composites: Part A* 77:1–25. doi:10.1016/j.compositesa.2015.06.007.

ISO (International Organization for Standardization). 1993. ISO 9613-1:1993 Acoustics - Attenuation of sound during propagation outdoors - Part 1: Calculation of the absorption of sound by the atmosphere.

ISO (International Organization for Standardization). 1998. ISO 10534-2:1998 Acoustics - Determination of sound absorption coefficient and impedance in impedance tubes - Part 2: Transfer-function method.

ISO (International Organization for Standardization). 2000. ISO 15186-1:2000 Acoustics - Measurement of sound insulation in buildings and of building elements using sound intensity - Part 1: Laboratory measurements.

ISO (International Organization for Standardization). 2003. ISO 354:2003 Acoustics - Measurement of sound absorption in a reverberation room.

Johnson, D. L., J. Koplik, and R. Dashen. 1987. Theory of dynamic permeability and tortuosity in fluid saturated porous media. *Journal of Fluid Mechanics* 176:379–402. doi:10.1017/S0022112087000727.

Jung, S. J., Y. T. Kim, Y. B. Lee, S. I. Cho, and J. K. Lee. 2008. Measurement of sound transmission loss by using impedance tubes. *Journal of the Korean Physical Society* 53 (2):596:600. doi:10.3938/jkps.53.596.

Kalauni, K., and S. J. Pawar. 2019. A review on the taxonomy, factors associated with sound absorption and theoretical modeling of porous sound absorbing materials. *Journal of Porous Materials* 26 (6):1795–819. doi:10.1007/s10934-019-00774-2.

Kesharwani, A. R., A. K. B. Bedi, and S. Bahl. 2020. Experimental study to measure the sound transmission loss of natural fibers at tonal excitations. *Materials Today: Proceedings. International Conference on Aspects of Materials Science and Engineering*. Chandigarh, India. doi: 10.1016/j.matpr.2020.04.839.

Kino, N. 2015. Further investigations of empirical improvements to the Johnson–Champoux–Allard model. *Applied Acoustics* 96:153–70. doi:10.1016/j.apacoust.2015.03.024.

Kino, N., and T. Ueno. 2008. Comparisons between characteristic lengths and fibre equivalent diameters in glass fibre and melamine foam materials of similar flow resistivity. *Applied Acoustics* 69 (4):325–31. doi:10.1016/j.apacoust.2006.11.008.

Komatsu, T. 2008. Improvement of the Delany-Bazley and Miki models for fibrous sound-absorbing materials. *Acoustical Science and Technology* 29 (2):121–29. doi:10.1250/ast.29.121.

Koruk, H. 2014. An assessment of the performance of impedance tube method. *Noise Control Engineering Journal* 62 (4):264–74. doi:10.3397/1/376226.

Koruk, H., and G. Genc. 2015. Investigation of the acoustic properties of bio luffa fiber and composite materials. *Materials Letters* 157:166–68. doi:10.1016/j.matlet.2015.05.071.

Lafarge, D., P. Lemarinier, J.-F. Allard, and V. Tarnow. 1997. Dynamic compressibility of air in porous structures at audible frequencies. *The Journal of the Acoustical Society of America* 102 (4):1995–2006. doi:10.1121/1.419690.

Lai, J. C. S., and M. Burgess. 1991. Application of the sound intensity technique to measurement of field sound transmission loss. *Applied Acoustics* 34 (2):77–87. doi:10.1016/0003-682X(91)90023-8.

Lalit, R., P. Mayank, and K. Ankur. 2018. Natural fibers and biopolymers characterization: A future potential composite material. *Journal of Mechanical Engineering* 68 (1):33–50. doi:10.2478/scjme-2018-0004.

Liao, J., S. Zhang, and X. Tang. 2020. Sound absorption of hemp fibers (cannabis sativa L.) based nonwoven fabrics and Composites: A review. *Journal of Natural Fibers* 1–13. doi:10.1080/15440478.2020.1764453.

Liuzzi, S., C. Rubino, P. Stefanizzi, and F. Martellotta. 2020. Performance characterization of broad band sustainable sound absorbers made of almond skins. *Materials* 13 (23):5474. doi:10.3390/ma13235474.

Mamtaz, H., M. H. Fouladi, M. Al-Atabi, and S. N. Namasivayam. 2016. Acoustic absorption of natural fiber composites. *Journal of Engineering* 5836107. doi:10.1155/2016/5836107.
Mechel, F. P. 2008. *Formulas of acoustics*. Berlin: Springer-Verlag.
Miki, Y. 1990. Acoustical properties of porous materials —modifications of Delany-Bazley models-. *Journal of the Acoustical Society of Japan (E)* 11 (1):19–24. doi:10.1250/ast.11.19.
Moussatov, A., C. Ayrault, and B. Castagnede. 2001. Porous material characterization - ultrasonic method for estimation of tortuosity and characteristic length using a barometric chamber. *Ultrasonics* 39 (3):195–202. doi:10.1016/S0041-624X(00)00062-7.
Norton, M. P., and D. G. Karczub. 2003. *Fundamentals of noise and vibration analysis for engineers*. 2nd ed ed. Cambridge, UK: Cambridge University Press.
Oldham, D. J., C. A. Egan, and R. D. Cookson. 2011. Sustainable acoustic absorbers from the biomass. *Applied Acoustics* 72 (6):350–63. doi:10.1016/j.apacoust.2010.12.009.
Progneaux, A., P. Bouillard, and A. Deraemaeker. 2015. A model updating technique based on the constitutive relation error for in situ identification of admittance coefficient of sound absorbing materials. *Journal of Vibration and Acoustics* 137 (5):051013. doi:10.1115/1.4030662.
Raj, M., S. Fatima, and N. Tandon. 2020. An experimental and theoretical study on environment-friendly sound absorber sourced from nettle fibers. *Journal of Building Engineering* 31:101395. doi:10.1016/j.jobe.2020.101395.
Sambu, M., M. N. Yahya, H. A. Latif, M. A. B. Roslan, and M. I. B. Ghazali. 2016. Influence of physical properties on the acoustical performance of the oil palm frond natural fibre. *ARPN Journal of Engineering and Applied Sciences* 11 (10):6458:64.
Santoni, A., P. Bonfiglio, P. Fausti, C. Marescotti, V. Mazzanti, F. Mollica, and F. Pompoli. 2019. Improving the sound absorption performance of sustainable thermal insulation materials: Natural hemp fibres. *Applied Acoustics* 150:279–89. doi:10.1016/j.apacoust.2019.02.022.
Shtrepi, L., and A. Prato. 2020. Towards a sustainable approach for sound absorption assessment of building materials: Validation of small-scale reverberation room measurements. *Applied Acoustics* 165:107304. doi:10.1016/j.apacoust.2020.107304.
Steffens, F., H. Steffens, and F. R. Oliveira. 2017. Applications of natural fibers on architecture. *Procedia Engineering* 200:317–24. doi:10.1016/j.proeng.2017.07.045.
Sydow, Z., and K. Bienczak. 2018. The overview on the use of natural fibers reinforced composites for food packaging. *Journal of Natural Fibers* 16 (8):1189–200. doi:10.1080/15440478.2018.1455621.
Taban, E., A. Khavanin, A. J. Jafari, M. Faridan, and A. K. Tabrizi. 2019b. Experimental and mathematical survey of sound absorption performance of date palm fibers. *Heliyon* 5 (6):e01977. doi:10.1016/j.heliyon.2019.e01977.
Taban, E., A. Khavanin, A. Ohadi, A. Putra, A. J. Jafari, M. Faridan, and A. Soleimanian. 2019a. Study on the acoustic characteristics of natural date palm fibres: Experimental and theoretical approaches. *Building and Environment* 161:106274. doi:10.1016/j.buildenv.2019.106274.
Taban, E., P. Soltani, U. Berardi, A. Putra, S. M. Mousavi, M. Faridan, S. E. Samaei, and A. Khavanin. 2020. Measurement, modeling, and optimization of sound absorption performance of kenaf fibers for building applications. *Building and Environment* 180:107087. doi:10.1016/j.buildenv.2020.107087.
Taban, E. A., T. M. Faridan, S. E. Samaei, and M. H. Beheshti. 2019c. Acoustic absorption characterization and prediction of natural coir fibers. *Acoustics Australia* 47 (1):67–77. doi:10.1007/s40857-019-00151-8.
Tadeu, A. J. B., and D. M. R. Mateus. 2001. Sound transmission through single, double and triple glazing. Experimental evaluation. *Applied Acoustics* 62 (3):307–25. doi:10.1016/S0003-682X(00)00032-3.
Tang, X., and X. Yan. 2017. Acoustic energy absorption properties of fibrous materials: A review. *Composites: Part A* 101:360–80. doi:10.1016/j.compositesa.2017.07.002.
Tarnow, V. 2002. Measured anisotropic air flow resistivity and sound attenuation of glass wool. *The Journal of the Acoustical Society of America* 111 (6):2735–39. doi:10.1121/1.1476686.
Wambua, P., J. Ivens, and I. Verpoest. 2003. Natural fibres: Can they replace glass in fibre reinforced plastics? *Composites Science and Technology* 63 (9):1259–64. doi:10.1016/S0266-3538(03)00096-4.
Wang, C.-N., Y.-M. Kuo, and S.-K. Chen. 2008. Effects of compression on the sound absorption of porous materials with an elastic frame. *Applied Acoustics* 69 (1):31–39. doi:10.1016/j.apacoust.2006.08.006.
Wang, X., F. You, F. S. Zhang, J. Li, and S. Guo. 2011. Experimental and theoretic studies on sound transmission loss of laminated mica-filled poly(vinyl chloride) composites. *Journal of Applied Polymer Science* 122 (2):1427–33. doi:10.1002/app.34047.
Wibisono, Y., C. R. Fadila, S. Saiful, and M. R. Bilad. 2020. Facile approaches of polymeric face masks reuse and reinforcements for micro-aerosol droplets and viruses filtration: A review. *Polymers* 12 (11):2516. doi:10.3390/polym12112516.
Xiang, H.-F., D. Wang, H.-C. Liu, N. Zhao, and J. Xu. 2013. Investigation on sound absorption properties of kapok fibers. *Chinese Journal of Polymer Science* 31 (3):521–29. doi:10.1007/s10118-013-1241-8.
Yang, T., L. Hu, X. Xiong, M. Petru, M. T. Noman, R. Mishra, and J. Militky. 2020. Sound absorption properties of natural fibers: A review. *Sustainability* 12 (20):8477. doi:10.3390/su12208477.

Yang, W., and L. Yan. 2012. Sound absorption performance of natural fibers and their composites. *Science China-Technological Sciences* 55 (8):2278:83. doi:10.1007/s11431-012-4943-1.
Zhu, X. D., B. J. Kim, Q. W. Wang, and Q. L. Wu. 2014. Recent advances in the sound insulation properties of bio-based materials. *Bioresources* 9:1764–86.